Desalination and Water Treatment
www.deswater.com
doi: 10.5004/dwt.2023.29633

297 (2023) 189–207
June

Polyaniline/banana peel composite: an eco-friendly adsorbent for removal of dihydrogen phosphate from groundwater

Abdullah A. Alotaibi[a], Abdulrahman F. Alharbi[a], Ahmed M.H. Ibrahim[a,b], Sami M. Abdel Azeem[a,c,*]

[a]*Department of Chemistry, College of Science and Humanities, Shaqra University, 11911, Saudi Arabia, email: sami_a@su.edu.sa (S.M. Abdel Azeem), aaalotaibi@su.edu.sa (A.A. Alotaibi), aalsaedi@su.edu.sa (A.F. Alharbi)*
[b]*Hot Laboratory Centre, Fuel Technology Department, Atomic Energy Authority, Abu-Zabal-Kalubia, P.O.: 13759, Egypt, email: a.ibrahim@su.edu.sa (A.M.H. Ibrahim)*
[c]*Chemistry Department, Faculty of Science, Fayoum University, Egypt, Tel.: +20 1207664342; Fax: +20 846370025; email: sma13@fayoum.edu.eg (S.M. Abdel Azeem)*

Received 14 October 2022; Accepted 14 May 2023

ABSTRACT

A low-cost polyaniline/banana peel (PAni/BP) composite was prepared by oxidative polymerization of aniline in the presence of agricultural waste BP powder and characterized by Fourier-transform infrared spectroscopy, scanning electron microscopy, X-ray diffraction, thermogravimetric analysis, and Brunauer–Emmett–Teller. The surface area and average pore width were 5.65 $m^2 \cdot g^{-1}$ and 61.2 nm, respectively. A maximum adsorption capacity of 56.8 $mg \cdot g^{-1}$ and more than 90% removal of 5.0 $mg \cdot L^{-1}$ phosphate, were achieved under optimized conditions. Phosphate adsorption is best described by the pseudo-second-order and Langmuir isotherm models. The Temkin isotherm gave an 8.2 $J \cdot mol^{-1}$ B constant, while the Dubinin–Radushkevich isotherm produced 14.1 $kJ \cdot mol^{-1}$ adsorption energy; both of them supported the chemisorption process. Thermodynamic parameters showed that the phosphate adsorption process was endothermic and spontaneous. For spiked groundwater, removal ranged between 90% and 95%, while desorbed phosphate removal ranged from 83% to 100%, with a relative standard deviation ranging from 2.0% to 7.4%.

Keywords: Polyaniline; Banana peel; Composite; Phosphate; Removal; Groundwater

1. Introduction

Environmental contamination is a serious and worldwide problem accompanied by rapid industrialization and urbanization in many countries. Recently, water pollution by phosphorus has become an important environmental issue associated with the eutrophication of water bodies due to the presence of an excess amount of phosphate [1].

Phosphate is the primary cause of eutrophication, which endangers humans, animals, and plants [2]. The runoff of phosphate can cause extreme algal growth and the production of microcystins in surface waters, which can be transported to drinking water and enter the food chain via irrigation, thereby affecting human health [3]. To prevent eutrophication, the United States Environmental Protection Agency (US-EPA) has stipulated that the total phosphate–phosphorus concentration should be less than 0.1 $mg \cdot L^{-1}$. If the level rose above this limit, it might result in quick algal blooms [4]. The presence of phosphate in various water resources is a growing phenomenon from a variety of sources. The two most dangerous sources are phosphate in sewage waters and traces of phosphate in treated sewage effluent. Furthermore, the use of fertilizer containing phosphate causes the latter to end up in groundwater as it

* Corresponding author.

dissolves and spreads in the irrigation water that runs off from agricultural fields [5].

In desert areas, the majority of the population relies solely on groundwater for agriculture and animal watering. Furthermore, desalination plants in these areas use groundwater as a raw water source. With the advancement of modern agricultural activities, many desert areas are now used for crop and fodder cultivation, necessitating the use of fertilizers in much greater quantities than before. During rain, the phosphate compounds dissolve and move into the ground, eventually collecting in underground water tanks. All of this contributed to the high phosphate concentration in the groundwater. Additionally, the potential for phosphate concern has been aided even in previously uninhabited areas due to the steady rise in the consumption of larger amounts of groundwater.

Although phosphate is not considered to be highly toxic, high concentrations cause eutrophication and the formation of algal blooms, which produce harmful cyanotoxins [6]. As a result, effective phosphate contamination removal from aquatic ecosystems is critical for public health and environmental sustainability.

Phosphate removal techniques currently available include biological treatment, chemical precipitation, ion exchange, membrane separation, and advanced oxidation processes. Even though these technologies are effective, they are also expensive and occasionally fall short. The majority of these techniques have certain drawbacks. Ion exchange and chemical precipitation both have issues with sludge disposal and/or high running costs. Biological treatment is limited to biodegradable pollutants, maintaining the sustainability of microbial growth. Membrane separation is expensive, and colloidal particles can irreversibly foul its surface. Due to high capital, operating, and maintenance costs, advanced oxidation processes are quite expensive. It also calls for the elimination of potentially harmful leftovers.

Adsorption has proven to be a viable strategy for phosphate removal owing to its straightforward methodology, low cost, high efficiency, ease of usage, and environmental friendliness. Additionally, it provides the option of adsorbent regeneration, often generates few byproducts, and removes phosphates even at low concentrations [7,8]. Materials with higher adsorption capacity, easier availability, and low costs are desirable.

Green adsorbents have been described in several biomaterials for the removal of phosphate (Table 1), such as sludge biochar [1], cotton stalk [9], pith carbon [10], sugarcane cellulose [11], wheat straw [12], peat [13], snail shell [14] and rice husk [15], algal biomass [16], giant reed [17], and sesame straw [18]. The equilibration periods of these biomaterials ranged from 15 to 80 min as shaking time, 3–24 h as contact time, and re-use cycles from 3 to 5. This communicates appropriate resilience against degradation, and the majority of these biomaterials are very inexpensive.

In terms of biodegradability, the developed composite belongs to the class of biodegradable conducting polymers that combine intrinsically conducting PAni polymers with the banana peel (BP) biodegradable carbohydrate biopolymers, namely starch. However, in aquatic environments such as freshwater and seawater, the biodegradability of starch-based biopolymers was less than that in soil, compost, or landfill [19]. This could be due to the limited number of organisms in these environments that can attach the composite structure. Thus, the proposed polyaniline/banana peel (PAni/BP) composite is anticipated to be a stable adsorbent material that could be used for several adsorption cycles.

Banana peel (BP) has been utilized to adsorb phosphate and chromate [20]. The BP biochar has been utilized to derive new adsorbents after modification with Fe_3O_4/zeolite imidazole framework (ZIF-67) for the adsorption of Cd [21]. The calcined magnetic BP biochar was reported for

Table 1
Green biomaterials reported on the removal/adsorption of phosphate

Biosorbent	Adsorption capacity, $mg \cdot g^{-1}$	Equilibration period	pH	Re-use cycles	Initial concentration, $mg \cdot L^{-1}$	Removal (%)	Adsorbent dose	Temp., °C	References
Sludge biochar	97.45	24[a]	2.2–4.3	–	153.3	90	2 $g \cdot L^{-1}$	25	[1]
Cotton stalk	51.54	15[b]	4.0–9–0	3.0	20–50	≥92	0.1 g/50 mL	20	[9]
Pith carbon	5.1	80[b]	3–10	–	10	79	0.3 g/ 50 mL	35	[10]
Sugarcane cellulose	18.9–21.4	60[b]	4.3–5.8	4.0	30	80	1 $g \cdot L^{-1}$	30	[11]
Wheat straw	45.7	3[a]	–	4.0	50	65	2 $g \cdot L^{-1}$	20	[12]
Peat	11.53	24[a]	2.0–5.0	–	25	99	1.0 g/80 mL	20	[13]
Snail shell	62.5–66.6	60	2–6	–	100	78.3	1.0 g/100 mL	30	[14]
Rice husks	63.99	24[a]	7.4	5.0	25–100	92–96	0.05 g/40 mL	25	[15]
Algal biomass	159.4	5[a]	5.0	5.0	10	98	0.05 g/50 mL	25	[16]
Giant reed	34.13	25[b]	4.0–9.0	–	50	80	0.1 g/50 mL	20	[17]
Sesame straw	116.58	12[a]	–	–	50	–	0.1 g/50 mL	25	[18]
PAni/BP	56.8	60[b]	5.5	10	5.0	92	0.1 g/20 mL	25	This work

[a]Contact time (h);
[b]Shaking time (min).

the adsorption of heavy metals [22], reactive black 5 [23], and phosphorus [24].

Polyaniline (PAni) composites are favorable materials due to their low costs, ease of synthesis, excellent environmental stability, and unique doping and de-doping properties [25,26]. PAni-based composites have also been widely studied for the adsorption of pollutants due to their high surface areas, excellent dispensability, and synergistic properties of the polymer and the filler [27]. Another advantage of PAni-based composites is their diverse morphological structures, which are adjustable by changing some synthesis parameters, such as the dopant type, reaction time, and temperature [28]. PAni-based composites with various nanostructures have been fabricated for removing heavy metals [29], phosphate [30], dyes [31,32], and perfluorinated compounds [33].

Many agro-wastes have been combined with PAni to obtain composite materials for the removal of pollutants from water, such as peanut husk [34] and *Tectona grandis* sawdust [35]. However, as far as we know, no work has been done to combine BP with PAni.

As a result, the leftover banana peel and the widely used, low-cost phosphate adsorbent (polyaniline) might be combined to create a biodegradable and incredibly cheap adsorbent with specialized adsorption capabilities. The potential to boost the capacity and selectivity of PAni by the addition of BP is an advantage anticipated from this composite, enabling the composite to have high adsorption capacity at low phosphate concentrations. All phosphate adsorbents have this as their major objective.

The present work describes the preparation of a new adsorbent by chemical bonding of PAni and BP to obtain the PAni/BP composite and investigates the removal of phosphate in groundwater with diverse total dissolved solids (TDS) values. To optimize the phosphate removal efficiency, the effect of pH, adsorbent dosage, contact time, and initial concentration on the adsorption capacity was studied.

2. Materials and methods

2.1. Instrumentation

A double beam UV-Vis spectrophotometer model Cintra 1010, operating with Cintra 2.4 Software (GBC Scientific Equipment, Braeside, Australia), was used for the determination of phosphate. A Carl Zeiss scanning electron microscope model Evo 15 (Jena, Germany) was used for imaging the surface of BP and the composite PAni/BP. Bruker FT-IR spectrometer model Vertex 70 (MA, USA), was used to record the spectra of banana peels using the KBr technique. The X-ray diffraction (XRD) patterns were made on a Shimadzu X-ray diffractometer model XRD-6000 (Kyoto, Japan) in the range of 2θ from 4° to 90° at room temperature. The Cu Kα was used as a radiation source with a wavelength (λ) of 0.15408 nm and other operating conditions include a scan rate of 8°min^{-1}, and an operating voltage and current of 50 kV and 40 mA, respectively. The TDS and electrical conductivity (EC) of the groundwater samples were measured using a Jenway Benchtop electrical conductivity meter model 4510 (Keison International Ltd., Chelmsford, UK). The instrument TDS measurement range and accuracy are 0–1,999 g·L^{-1} and 0.5% ± 2 digits, respectively. Thermogravimetric analysis (TGA) was made on a Shimadzu TGA-51/51H analyzer using a composite weight of 10.14 mg and a heating rate of 10°C min^{-1}. The surface area and porosity of the PAni/BP composite were determined with the Brunauer–Emmett–Teller (BET) approach using a low-temperature N_2 gas adsorption–desorption technique operated on the Micromeritics® TriStar II Plus analyzer model 2390t V2.03 (GA, USA) of surface area and pore size analyzer at 77 K. Stuart orbital mechanical shaker model S1500 (London, UK), with a speed of 30–300 rpm, was used to shake the samples. Double-distilled water used throughout the study was obtained from a purification system (Hamilton Glass Ltd., Margate, UK). Qualitative filter paper No. 101 (Dorsan Filtration SL Co., Barcelona, Spain) was used to filter the extracts. Glass bottles with Teflon caps were used for the adsorption study. Cellulose acetate membrane filters with a 0.45 μm pore size were used for collecting the eluate after the desorption process.

2.2. Reagents

Sodium dihydrogen orthophosphate $NaH_2PO_4{\cdot}2H_2O$, aniline solution, ammonium peroxydisulfate (APS) or $(NH_4)_2S_2O_8$, and hydrochloric acid were purchased from Techno Pharmchem Co. (Haryana, Delhi, India). Sulfuric acid was obtained from CDH Co., (New Delhi, India). Ammonium molybdate tetrahydrate $(NH_4)_6Mo_7O_{24}{\cdot}4H_2O$ (Suvachem Company, Maharashtra, India), and ascorbic acid (BDH Chemical Ltd., Dorset, UK), were analytical reagents grade. A standard phosphate solution of 100 mg·L^{-1} was prepared by dissolving 0.164 g $NaH_2PO_4{\cdot}2H_2O$ in distilled water and then making it up to 1 L. A working solution of 10 mg·L^{-1} was obtained by dilution from the standard solution. Ammonium molybdate solution was prepared by dissolving 20 g in 500 mL of distilled water and leaving it to stand until complete dissolution. The ascorbic acid solution was prepared by dissolving 1.32 g of reagent in 75 mL of double-distilled water. A 2.5 mol·L^{-1} sulfuric acid was prepared by diluting 70 mL of the concentrated acid up to 500 mL with distilled water. The phosphate reagent was prepared by mixing sulfuric acid (125 mL), ammonium molybdate (37.5 mL), and ascorbic acid (75 mL). The yellow-colored reagent was prepared daily and used for no more than 24 h.

2.3. Synthesis of PAni/BP composite

The BP powder was prepared from mature and fresh banana fruit peels obtained from a local market. The peels were washed several times with distilled water to remove the dust. It was sliced into small pieces and dried at 110°C to a constant weight. The dried material was ground in a porcelain mortar and sieved with 0.5–1.0 mm diameter.

The PAni/BP composite was synthesized by *in-situ* polymerization of aniline with an APS oxidant in the presence of BP powder according to the modified method [36] as follows: 10 g of BP were added to 250 mL of 1 mol·L^{-1} of HCl and stirred very well. Then, 2.0 mL aniline was added to the suspension and stirred for 30 min at room temperature. Another solution containing 6.0 g APS was dissolved in 100 mL of 1.0 mol·L^{-1} HCl. Both solutions were cooled to 4°C. After that, the APS was gradually added to the

suspension over 60 min while the reaction mixture was vigorously stirred. Soon after, a dark green suspension of PAni/BP composite was formed and then kept for 24 h under stirring. After filtering the crude solid, it was washed with distilled water several times until the washings were clear and neutral. The dark green powder from the PAni/BP composite was left to dry at ambient temperature and stored for further adsorption studies. The proposed chemical structure and the adsorption reactions of PAni/BP with phosphate are shown in Fig. 1.

At pH 5.5, the predominant species is the monovalent dihydrogen form of phosphate, $H_2PO_4^-$ [37]. Adsorption can take place via electrostatic attraction to the protonated imine nitrogen in PAni. Also, the protonated OH and C=O in carbohydrates, phenolic acids, flavanones, and flavonols, as well as the NH_2 groups in the amino acids (leucine, valine, phenylalanine, and threonine) in BP [38].

The potassium chloride solid addition method was used to establish the point of zero charges (pH_{zpc}) of the PAni/BP composite [39]. A total of 50 mL of 0.1 mol·L^{-1} KCl portions were adjusted to pH 2, 4, 6, 8, and 10 using 0.1 mol·L^{-1} solutions of HCl and NaOH. Each portion received 0.01 g of the composite, which was then left at room temperature for 24 h. A pH meter was used to measure both the initial and final pH readings. Evaluation of pH_{zpc} was made possible by plotting the pH change ($\Delta pH = pH_f - pH_i$) against the starting pH and finding the intersection point where $\Delta pH = 0$.

2.4. Adsorption procedure

Adsorption parameters involving the adsorbent dose, sample pH, contact time, and extraction isotherm were studied. A 20 mL phosphate solution at a concentration of 5.0 mg·L^{-1} phosphate was placed in a glass bottle, and Teflon caps were then mixed with 0.1 g sorbent. The 0.1 mol·L^{-1} solution of HCl and NaOH were used to adjust the solution to pH 5.5. The mixture was shaken for 1 h at a speed of 250 rpm. After extraction, the composite was separated by filtration using filter paper, and 10 mL of the filtrate was analyzed for phosphate content by the recommended ammonium molybdate method. A kinetic study was carried out by taking a fixed concentration of the phosphate solution (*ca.* 5.0 mg·L^{-1}) and mixing it with 0.1 g of the composite, then shaking it from 2 to 60 min at room temperature. An aliquot of 20 mL from the solution phase was taken after filtration, and the remaining phosphate was determined. The removal efficiency (%) and the amount adsorbed at equilibrium (Q_e, mg·g^{-1}) of phosphate were calculated using Eqs. (1) and (2).

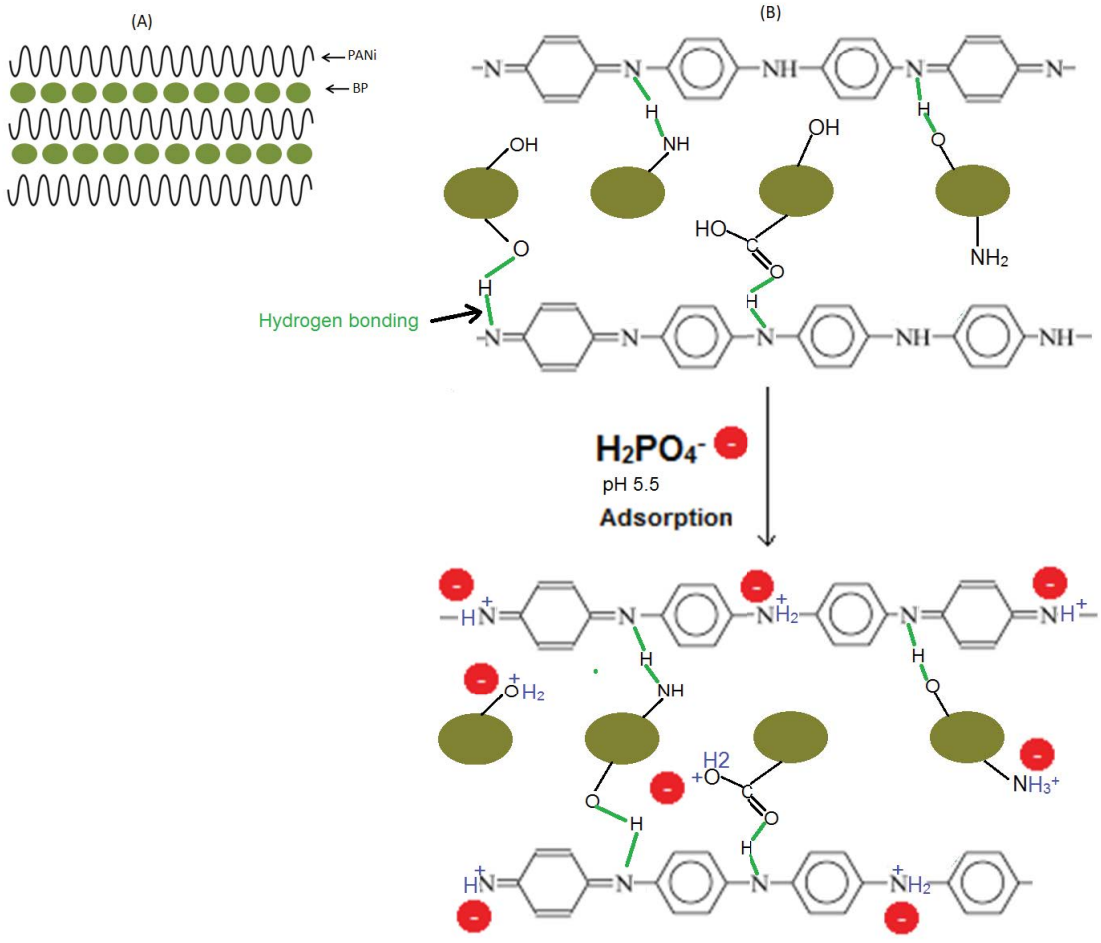

Fig. 1. Proposed layer arrangement in PAni/BP composite (A), the interaction between BP surface groups and PAni (B).

$$\text{Removal}(\%) = \left[\frac{(C_o - C_e)}{C_o}\right] \times 100 \quad (1)$$

$$Q_e = \left[\frac{(C_o - C_e)V}{m}\right] \quad (2)$$

where C_o and C_e are the initial and equilibrium concentrations of KH_2PO_4 (mg·L^{-1}), respectively. V is the sample volume (L), and m is the mass of the adsorbent (g).

Adsorption isotherm experiments were conducted by varying the initial concentration of phosphate from 1.0 to 200 mg·L^{-1} with a fixed PAni/BP amount of 0.1 g and a solution pH of 5.5 at 25°C. After adsorption, the amount of phosphate remaining in the supernatant solution was determined.

2.5. Phosphate determination

A spectrophotometric determination of phosphate was carried out according to the recommended method for natural waters [40]. In this context, the calibration curve was obtained by serial dilution of stock solution with deionized water to yield a final phosphate concentration ranging from 0.5 to 20 mg·L^{-1}. In a 25-mL calibrated flask, 20 mL of the phosphate solution was mixed with 4.0 mL of the ammonium molybdate mixed reagent, and the solution was completed with distilled water. A blue color develops slowly, indicating the phosphomolybdenum blue complex. After 20 min, the absorbance was measured at 830 nm against a reagent blank. The standard curve was obtained by unweighted linear regression of the absorbance (A) vs. phosphate concentration (C, mg·L^{-1}). The linear regression equation was: $A = 0.055C + 0.009$ ($R^2 = 0.993$). The un-weighed equation was used to calculate the concentration of phosphate in the analyzed samples.

2.6. Groundwater samples

The groundwater samples numbered G ≠ 1, G ≠ 2, G ≠ 3, G ≠ 4, and G ≠ 5 were collected from different locations in Al-Kuwait governorate, Riyadh region, Kingdom of Saudi Arabia (KSA). The physico-chemical properties of the examined samples are presented in Table 2. The TDS of the selected samples ranged from 202 to 3040 mg·L^{-1} with the order G4 > G5 > G3 > G2 > G1. Fig. S1 shows an image of the measurement of groundwater TDS. This indicates the great diversity in the types of groundwater in the studied region. This depends on the amount of phosphate found in the rock (inorganic phosphates) through which the well was dug and the agricultural activities around it. Also, the phosphate content varied from 1.1 to 2.6 mg·L^{-1} which is higher than the World Health Organization (WHO) standards, typically 0.1 mg·L^{-1} [41]. All samples were filtered through a 0.45 μm membrane filter, acidified with nitric acid to pH 2, and directly analyzed. A 20 mL aliquot of raw water was spiked with the concentrations of 0.0, 3.0, and 5.0 mg·L^{-1} phosphate and adjusted to pH 5.5, then mixed with 0.1 g sorbent and shaken for 1 h at 25°C. The retained amount was desorbed by shaking the composite with 5 mL of a 0.15 mol·L^{-1} sodium hydroxide solution and was measured with the ammonium molybdate spectrophotometric method.

3. Results and discussion

3.1. Characterization of PAni/BP composite

The Fourier-transform infrared (FT-IR) spectra of BP and PAni/BP composite are shown in Fig. 2.

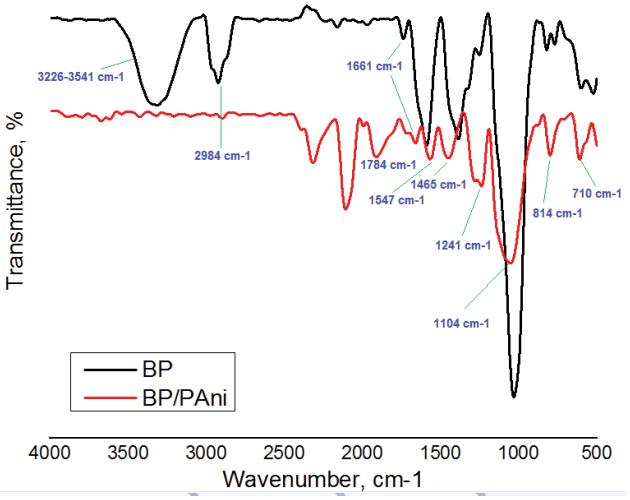

Fig. 2. Fourier-transform infrared spectra of BP (A) and PAni/BP composite (B).

Table 2
Influence of the physico-chemical parameters of the studied groundwater samples on the phosphate removal using PAni/BP composite

Sample	Physico-chemical properties of groundwater									Removal (%)
	pH	Conductivity, μS·cm^{-1}	TDS, mg·L^{-1}	Cl^-, mg·L^{-1}	SO_4^{2-}, mg·L^{-1}	NO_3^-, mg·L^{-1}	PO_4^{3-} mg·L^{-1}	Ca, mg·L^{-1}	Mg, mg·L^{-1}	
G ≠ 1	8.0	337	202	71	28	12	2.0	200	19	95
G ≠ 2	7.8	1,469	881	355	49	14.5	1.1	100	50	90
G ≠ 3	7.5	2,150	1,288	320	115	9.3	1.8	124	96	91
G ≠ 4	7.4	5,066	3,040	887	184	13.7	2.3	408	65	93
G ≠ 5	7.7	4,080	2,441	710	161	11.2	2.6	292	122	90

In the PAni/BP spectra, two characteristic bands that appeared at 1,465 and 1,547 cm^{-1} were assigned to the benzenoid and quinoid rings that confirmed the emeraldine structure of PAni. The weak band at 1,241 cm^{-1} is assigned to the C–N stretching of the primary and secondary vibrations in PAni. Evidentially, an absorption band appeared at 1,784 cm^{-1} assigned to the C=O group of the BP portion in the composite. The bands at 814 and 710 cm^{-1} are assigned for the out-of-plane 1,4-disubstituted benzene ring in PAni. In both spectra of BP (a) and PAni/BP composite (b), two characteristic bands appeared at 1,104; 1,661 and 2,986 cm^{-1} assigned for the C–O–C, C=N, and aromatic C–H stretching, respectively. Moreover, the broadband from 3,226 to 3,541 cm^{-1} corresponding to COOH and OH stretching in the BP spectrum nearly disappeared in the PAni/BP spectrum (b) which might be due to their involvement in the polymerization of aniline and also due to the coating of part of the BP surface with PAni. Finally, the developed composite contains positively charged adsorption sites that facilitate the adsorption of phosphate anions.

The scanning electron microscopy (SEM) of the BP and the developed PAni/BP composite are shown in Fig. 3. An inhomogeneity of the surface morphology of BP and PAni/BP was observed. The BP image depicted an irregular structure and high porosity with macropores, with dimensions ranging from 60–100 μm. The PAni/BP composite, on the other hand, demonstrated a significant change in pore structure after PAni polymer implantation, with the surface becoming smoother and the pore diameter becoming smaller. Regardless, the surface remained irregular, increasing the ultimate surface area available for phosphate adsorption.

The XRD pattern of BP and PAni/BP composite in the 2θ range from 5°–90° are presented in Fig. 4.

Both patterns seem to be very similar and characteristic of amorphous materials. The BP pattern showed three strongest peaks at 2θ of 4.30°, 16.46°, and 20.28°. While the

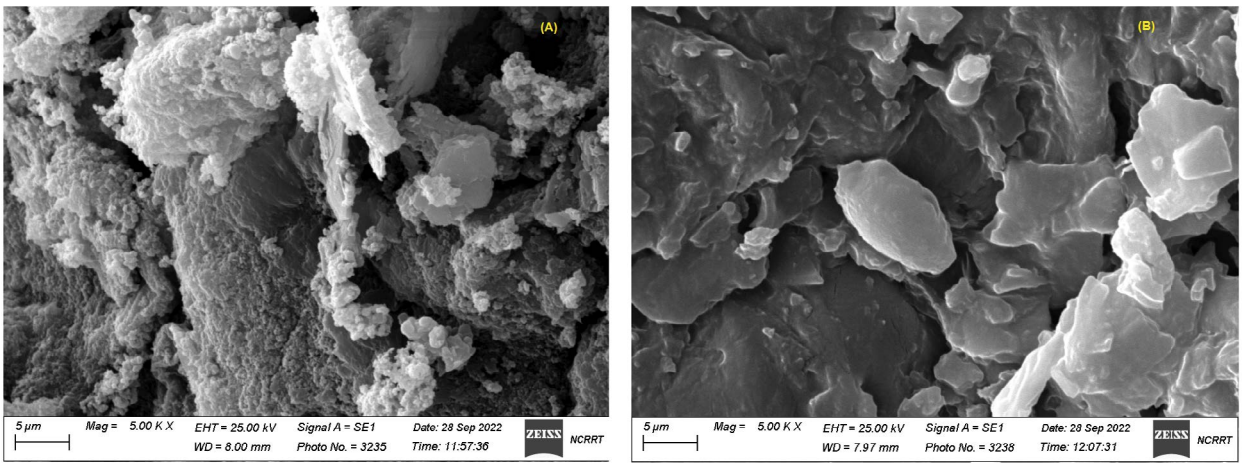

Fig. 3. Scanning electron micrographs of BP (A) and PAni/BP composite (B).

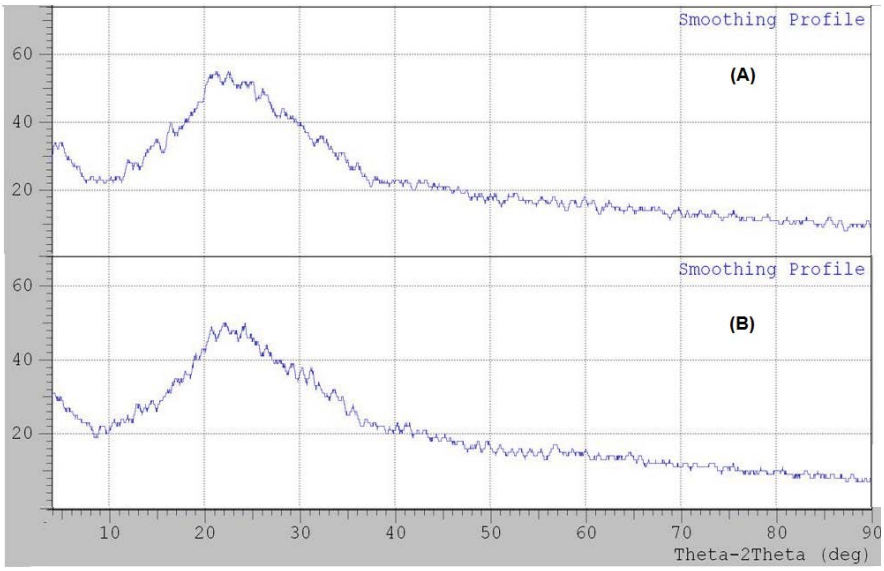

Fig. 4. X-ray diffraction patterns of raw BP (A) and PAni/BP composite (B).

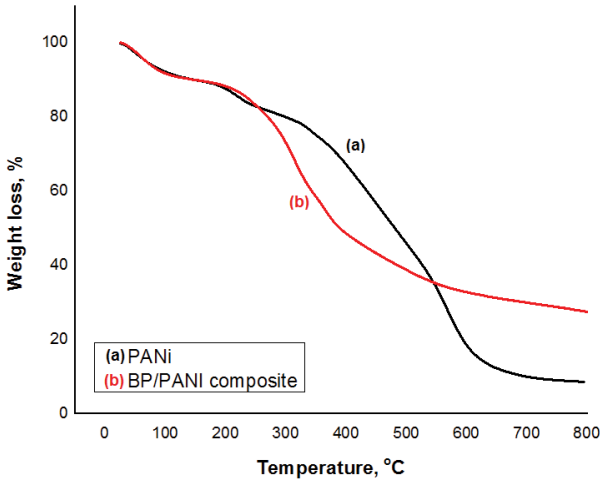

Fig. 5. Thermogravimetric profiles of PAni (a) and PAni/BP composite (b).

PAni/BP composite presented diffraction peaks at 20.44°, 20.76°, and 22.16°. The position of these peaks has indicated the amorphous structure of BP and also the PAni polymer had an amorphous crystalline in the PAni/BP composite.

The TGA profiles of the BP/PAni composite and PAni are displayed in Fig. 5. For the PAni/BP composite, there was about 10% weight loss before 130°C, which may have been caused by the loss of adsorbed water and volatile compounds. Also, a significant weight loss of 42% from 240°C to 400°C may have been caused by the elimination of higher oligomers from PAni and BP materials. Then, between 400°C and 600°C, there was a 16% weight loss that may be due to the oxidative decomposition of BP and PAni into several organic degradation products, including ammonia, aniline, ethylene, and acetylene [36]. Following that, the 5% loss from 600°C to 800°C continues for a prolonged time, which may be caused by the production of combustion gases like CO and CO_2 [1]. When PAni was used alone, the deterioration occurred more quickly from 385°C to 600°C, with a mass loss of about 60%. Thus, the PAni/BP composite demonstrated greater thermal resilience against oxidative decomposition.

The N_2 adsorption–desorption isotherm onto PAni/BP is shown in Fig. 6A.

Type IV adsorption–desorption isotherm, which is typical of mesoporous materials. Adsorption–desorption isotherms of type IV were obtained, which is typical of mesoporous materials with micro and macroporous structures. The BET surface area of PAni/BP composite before and after $H_2PO_4^-$ adsorption from 10 mg·L^{-1} solution was calculated using the multipoint BET model. The BET surface area of PAni/BP was 5.65 m^2·g^{-1}, the pore volume was 0.0866 cm^3·g^{-1}, and the average pore size was 61.2 nm. After $H_2PO_4^-$ adsorption, they were 4.47 m^2·g^{-1}, 0.022 cm^3·g^{-1}, and 35.6 nm, respectively. Because of the phosphate filling the micropores, the surface area was greater than after adsorption. The composite porosity can be categorized following its overall porosity. They can be classified as macropores (d > 50 nm), mesopores (2 < d < 50 nm), or micropores (d < 2 nm). The pore-size distribution before and after $H_2PO_4^-$ adsorption is shown in Fig. 6B.

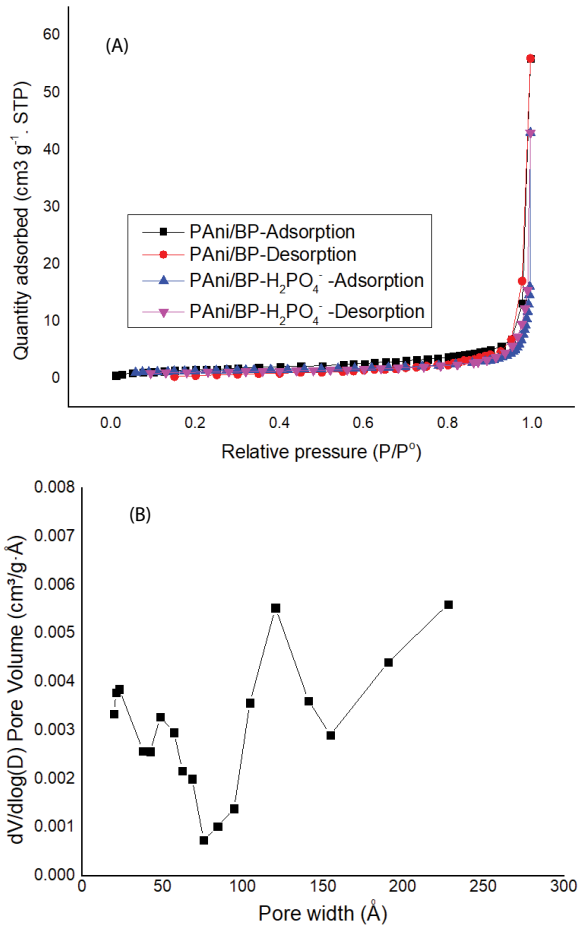

Fig. 6. (A) N_2 adsorption–desorption isotherm of PAni/BP composite and after adsorption of 10 mg·L^{-1} KH_2PO_4 at pH 5.5 and (B) pore-size distribution of PAni/BP composite.

3.2. Adsorption study

3.2.1. Sample pH

The effect of solution pH on the adsorption of phosphate was studied in the range 2–9 using a 10 mL sample containing 5.0 mg·L^{-1} phosphate, 0.1 g adsorbent, and a shaking period of 1 h. The obtained results are shown in Fig. 7A.

The optimal pH for phosphate removal was 5–6, with maximum removal of 92% achieved. When the pH goes down from 5, the removal (%) decreases rapidly, which might be due to the competition of hydrogen ions for the active sites. At pH values higher than 6, removal decreases gradually, which might be due to the compensation of protons with the excess hydroxyl groups in the alkaline environment. According to the study of the pH of the point of zero charges (pH_{zpc}) presented in Fig. 7B, the estimated pH_{zpc} value was found at pH 5.3. Thus, there was an anion repulsion between the negatively charged surface of the adsorbent and the phosphate. This confirmed the strong effect of the electrostatic attraction forces on adsorption. Therefore, the sample was adjusted to pH 5.5 in the subsequent adsorption study. According to the dissociation constants of phosphoric acid, they are pK_{a1} 2.2, pK_{a2} 7.2, and

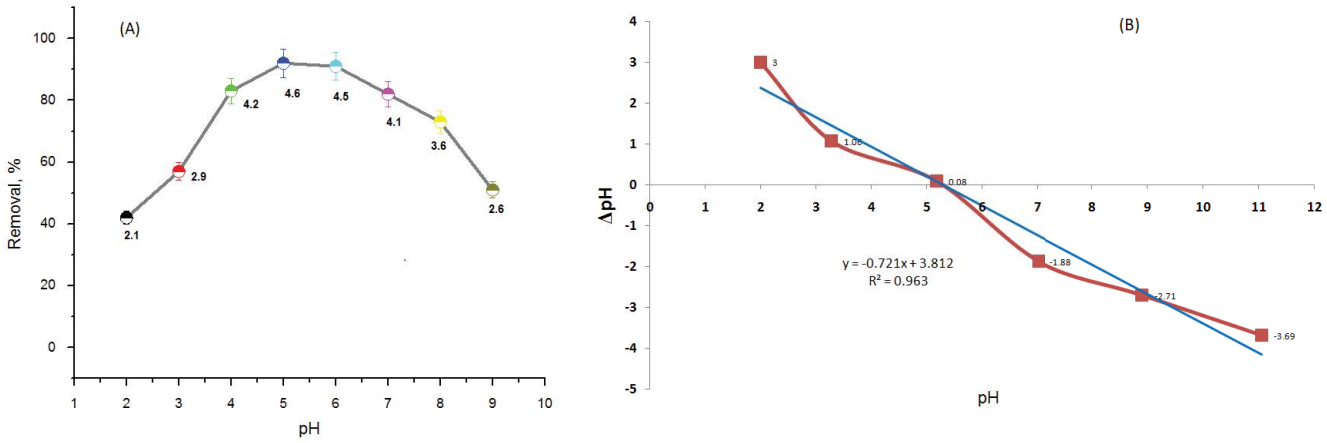

Fig. 7. (A) Influence of sample pH on the removal of phosphate with PAni/BP composite initial phosphate ($H_2PO_4^-$) concentration: 5.0 mg·L^{-1}, shaking time: 60 min, adsorbent weight: 0.1 g, sample volume: 20 mL, 25°C. (B) Determination of pH_{zpc} using KCl solid addition method: 0.01 g PAni/BP, 50 mL 0.1 mol·L^{-1} KCl, 24 h, 25°C.

pK_{a3} 12.3. Therefore, when the pH is between 3.0 and 7.2, monovalent $H_2PO_4^-$ is the dominant species in solution, and at pH between 7.2 and 11.0, the divalent species HPO_4^{2-} is the dominant phosphate [42].

This indicates the adsorbent surface is positively charged at pH values lower than 6, which might be due to the protonation of the composite's amino, imino, hydroxyl, and carboxylic groups into $-NH_3^+$, $-^+NH=$, and $-OH_2^+$, and $-COOH_2^+$ facilitating the dihydrogen phosphate anion attraction. When the pH was raised above the pH_{zpc} of 5.3, the PAni/BP surface became negatively charged and the $H_2PO_4^-$ repulsion increased.

3.2.2. Kinetic study

Shaking time was studied in the range of 1–60 min at a pH of 5.5 and a phosphate concentration of 5.0 mg·L^{-1}. The results obtained are presented in Fig. 8.

The removal increased rapidly within the first 20 min. Equilibration was attained after 40 min of shaking which indicates fast sorption of phosphate and good accessibility of adsorption sites to the target analyte. The maximum removal reached 92% after 60 min of shaking. Therefore, to ensure the achievement of equilibration, a 60 min shaking period was established in the subsequent experiments.

The kinetic mechanism governing the adsorption process was studied by fitting experimental results to the pseudo-first-order, pseudo-second-order, and intraparticle diffusion models. The validity of the pseudo-first-order model could be examined by plotting log ($Q_e - Q_t$) vs. t, where Q_e and Q_t represent the adsorbed amount of phosphate (mg·g^{-1}) at equilibrium and at any time t (min), respectively. Lagergren and Kungliga [43] expressed the pseudo-first-order rate as Eq. (3):

$$\ln\left(Q_e - Q_t\right) = \ln Q_e - k_1 t \tag{3}$$

As shown in Table 3, the regression analysis results show a linear correlation coefficient (R^2) of 0.983 (Fig. 9A). The calculated Q_e value was 3.17 mg·g^{-1}, with a very significant discrepancy with the experimental Q_{exp} value of 2.31 mg·g^{-1},

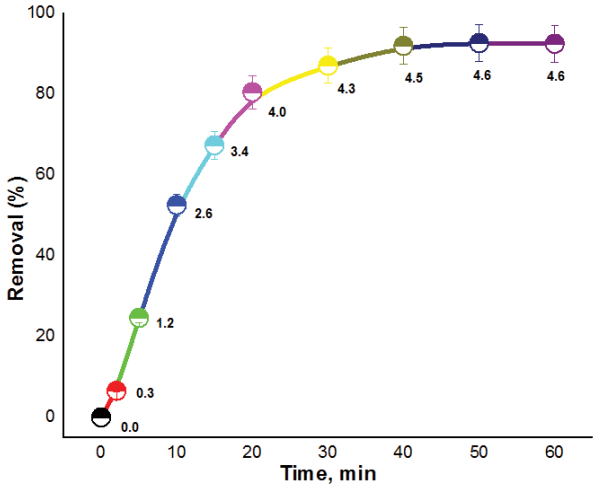

Fig. 8. Effect of shaking time on the phosphate removal by PAni/BP composite: initial phosphate ($H_2PO_4^-$) concentration: 5.0 mg·L^{-1}, pH = 5.5, adsorbent weight: 0.1 g, sample volume: 20 mL, 25°C.

Table 3
Adsorption kinetic data for phosphate (5.0 mg·L^{-1} KH_2PO_4, pH 5.5) adsorption onto PAni/BP composite

Kinetic model	Parameter	
Experimental	$Q_{e,exp}$, mg·g^{-1}	2.31
	$Q_{e,cal}$, mg·g^{-1}	3.17
Pseudo-first-order model	k_1, min^{-1}	0.124
	R^2	0.983
	$Q_{e,cal}$, mg·g^{-1}	2.83
Pseudo-second-order model	k_2, mg^{-1}·min^{-1}	0.029
	R^2	0.992
	k_{id}, mg^{-1}·g^{-1}·min$^{-1/2}$	0.616
Intraparticle diffusion model	R^2	0.994
	C, mg·g^{-1}	0.711

showing that the pseudo-first-order model is inconvenient for describing the adsorption kinetics results. The pseudo-second-order suggested by Ho et al. [44] is expressed by Eq. (4):

$$\frac{t}{Q_t} = \frac{1}{\left(k_2 Q_e^2\right)} + \left(\frac{1}{Q_e}\right)t \tag{4}$$

where k_2 is the pseudo-second-order rate constant (mg·g^{-1}·min^{-1}). Fig. 9B depicts a plot of the experimental results with this model. The R^2 values obtained from the slope of the regression equations are greater than those derived from the pseudo-first-order model; with values of 0.992. Furthermore, the calculated Q_e value from the second-order model was remarkably similar to the experimental value of Q_e. This verified that the pseudo-second-order model is appropriate for investigating the experimental kinetic effects.

The intraparticle diffusion model was applied to data of different initial phosphate concentrations for further investigation of the adsorption behavior. The Morris–Weber Eq. (5) was used to investigate the intraparticle diffusion behavior [45].

The slope of the plot of Q_t values versus the square root of shaking time t was used to evaluate the intraparticle diffusion rate constant k_{id} (mg·g^{-1}·min$^{-1/2}$).

$$Q_t = k_{id} t^{1/2} + C \tag{5}$$

where C (mg·g^{-1}) is a constant describing the boundary layer effect. The plots have two linear stages. Firstly, a linear relationship with higher slopes at the beginning intervals was a rapidly increasing step. As can be seen in Fig. 9C, the straight lines did not pass through the origin, indicating that a film diffusion phase occurred during the initial adsorption stages and intraparticle diffusion contributes to the rate-limiting step. The intraparticle diffusion model described by the

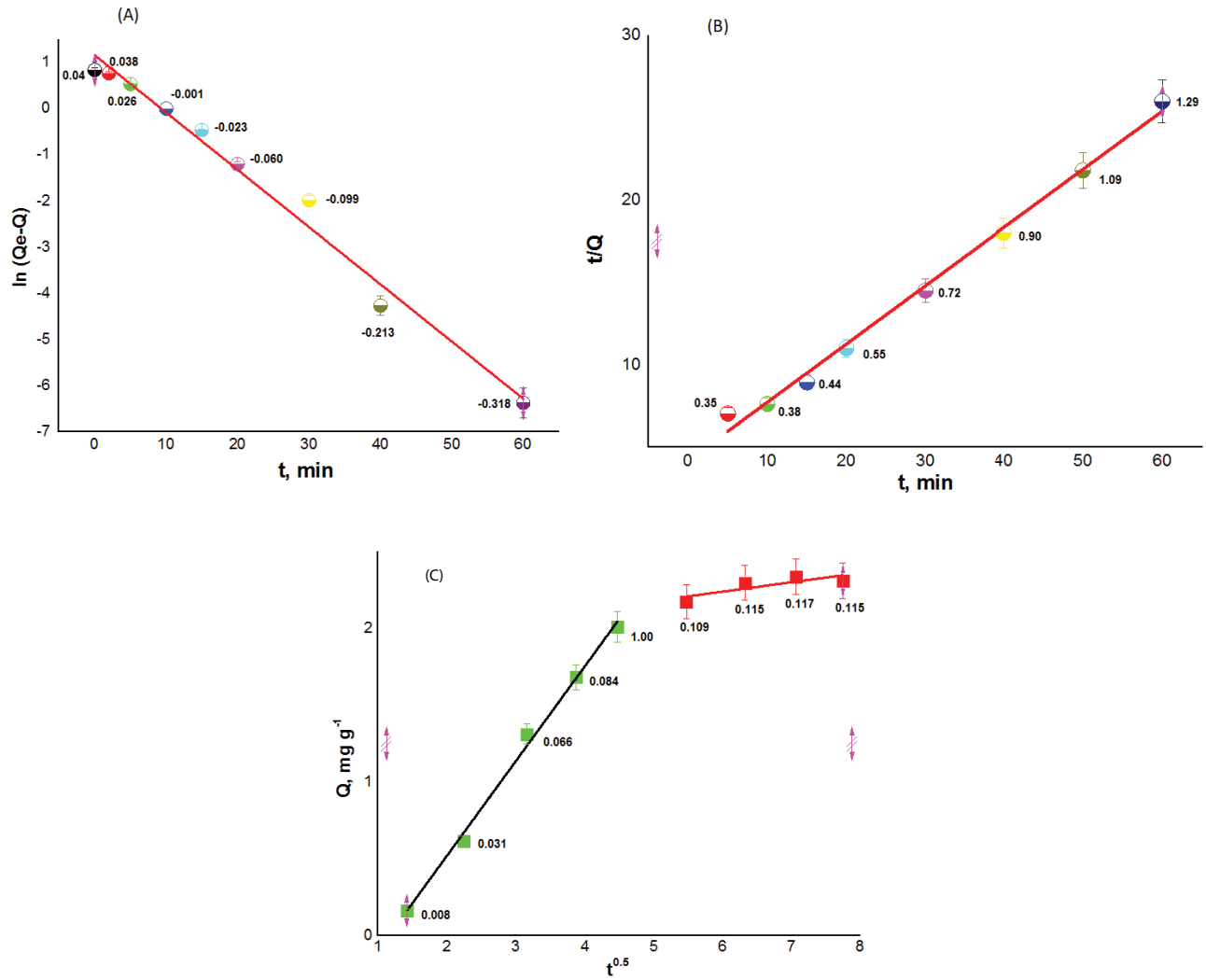

Fig. 9. Pseudo-first-order (A) and pseudo-second-order (B): initial phosphate ($H_2PO_4^-$) concentration: 5.0 mg·L^{-1}, pH = 5.5, adsorbent weight: 0.1 g, sample volume: 20 mL, 25°C. (C) Plotting of the intraparticle diffusion model for adsorption of 5.0 mg·L^{-1} of $H_2PO_4^-$, pH = 5.5, adsorbent weight: 0.1 g, sample volume: 20 mL, 25°C.

Morris–Weber Eq. (5) is applied only at the initial adsorption stages. For this stage, the calculated R^2 value was 0.994, respectively, and the k_{id} value was 0.616 mg·g^{-1}·min$^{-1/2}$.

Secondly, a successive linear stage had a lower slope of 0.0613 with a ten-fold reduction in the diffusion rate. This suggested a multistep adsorption mechanism with a relatively slow increase in the quantity adsorbed and stagnation afterward. The first stage denotes the diffusion of phosphate molecules to the adsorption sites, while the second one is ascribed to equilibrium. None of the obtained linear plots passed through the original point, representing the fact that the intraparticle diffusion was not the sole rate-controlling step of the removal [46].

3.2.3. Adsorption isotherm

The adsorption isotherm was investigated at concentrations ranging from 1.0 to 200 mg·L^{-1}, 0.1 g adsorbent dose, and a 20 mL sample volume optimized at pH 5.5 (Fig. 10A). At equilibrium, the value of Q_e increased rapidly at lower concentrations as the initial concentration of phosphate was increased, which reveals the gradual saturation of the sorbent binding sites. This could be due to a greater likelihood of collision between phosphate and the adsorbent surface, as well as a higher concentration gradient, which increases the rate of mass transfer [47]. When all binding sites have been entirely occupied, no further adsorption occurs, and the isotherm reaches a plateau.

The maximum monolayer adsorption capacity (Q_{max}, mg·g^{-1}) was calculated from the Langmuir model. The adsorption capacity depends strongly on the binding strength to the composite, which in turn depends on the degree of protonation–deprotonation in both BP and PAni. The results also indicate that phosphate is directly attached to the composite by using donor atoms in the PAni and BP polymers [48]. The value of Q_{max} obtained was 56.8 mg·g^{-1} which is better than that of other PAni-based composites such as PAni/La [30] and PAni/TiO_2 [49,50] but less than that of PAni/$Ni_{0.5}Zn_{0.5}Fe_2O_4$ [48]. The exhibited higher adsorption capacity of PAni/BP can be attributed to the presence of different adsorption mechanisms, including the formation of monodentate and bidentate phosphate surface complexes and electrostatic interactions with the positively charged active sites [50]. In addition, the phosphate transfer into the narrow pores in the composite bulk would greatly increase the rate of phosphate accumulation in the solid phase, permitting a faster adsorption rate.

The adsorption process begins with phosphate diffusion from the bulk of the solution to the sorbent surface, then to the inner surface to combine with active groups for ultimate accumulation in a monolayer or extended to a multilayer pattern. The analysis of isothermal data is essential to develop an equation that accurately describes the adsorption mechanism. Langmuir and Freundlich adsorption isotherms were used to fit the experimental results. The Langmuir isotherm [51] was examined for its ability to match the experimental results; it is defined by Eq. (6).

$$\frac{C_e}{Q_e} = \frac{C_e}{Q_{max}} + \frac{1}{Q_{max}K_L} \tag{6}$$

where Q_{max} is the maximum adsorption capacity of phosphate (mg·g^{-1}) to form a complete monolayer. C_e is the equilibrium concentration of phosphate (mg·L^{-1}) and K_L is the Langmuir constant related to the affinity of binding sites for phosphate.

The Freundlich isotherm [52] is an empirical model for heterogeneous adsorption that is presented by Eq. (7).

$$\ln Q_e = \left(\frac{1}{n}\right)\ln C_e + \ln K_F \tag{7}$$

where K_F and n are the Freundlich constants related to adsorption capacity and intensity, respectively.

The Temkin isotherm model [53], described by Eq. (8), was applied to describe and evaluate the heat of adsorption and the adsorbent–adsorbate interaction.

$$Q_e = B\ln A_T + B\ln C_e \tag{8}$$

where A_T is the Temkin isotherm equilibrium binding constant (L·g^{-1}) and B is the heat of adsorption (J·mol^{-1}).

Dubinin–Radushkevich's isotherm model doesn't assume a constant sorption potential or homogeneous surface [54]. The Dubinin–Radushkevich model is represented by Eq. (9):

$$\ln Q_e = \ln X_m - \beta\varepsilon^2 \tag{9}$$

By plotting $\ln Q_e$ vs. ε^2 the values of slope (β) and intercept ($\ln X_m$) can be obtained, where X_m (mol·g^{-1}) is the maximum adsorbed amount of phosphate onto 1 g of the composite. The constant β (mol^2·J^{-2}) represents the sorption energy. The Polanyi potential (ε) can be calculated by using Eq. (10):

$$\varepsilon = RT\ln\left(1+\frac{1}{C_e}\right) \tag{10}$$

where R (8.314 J·mol^{-1}·K^{-1}) is the gas constant and T is the absolute temperature of 298 K.

The free energy of adsorption E (kJ·mol^{-1}) is nominated as the free energy change when one mole of phosphate is transferred from the solution infinity to the surface of the composite adsorbent. It can be calculated using Eq. (11):

$$E = \frac{1}{\sqrt{-2\beta}} \tag{11}$$

The isotherm models for Langmuir, Freundlich, Temkin, and Dubinin–Radushkevich are shown in Fig. 10B–E.

Based on isotherm results listed in Table 4, the correlation coefficients (R^2) for Langmuir and Freundlich were 0.998 and 0.967, respectively. Thus, the Langmuir model was better to describe the experimental results, and the process is a monolayer chemical adsorption. This could be emphasized by the kinetic results that followed the second-order kinetic model. The calculated values of Q_{max} and K_L from the Langmuir model were found to be 56.8 mg·g^{-1} and

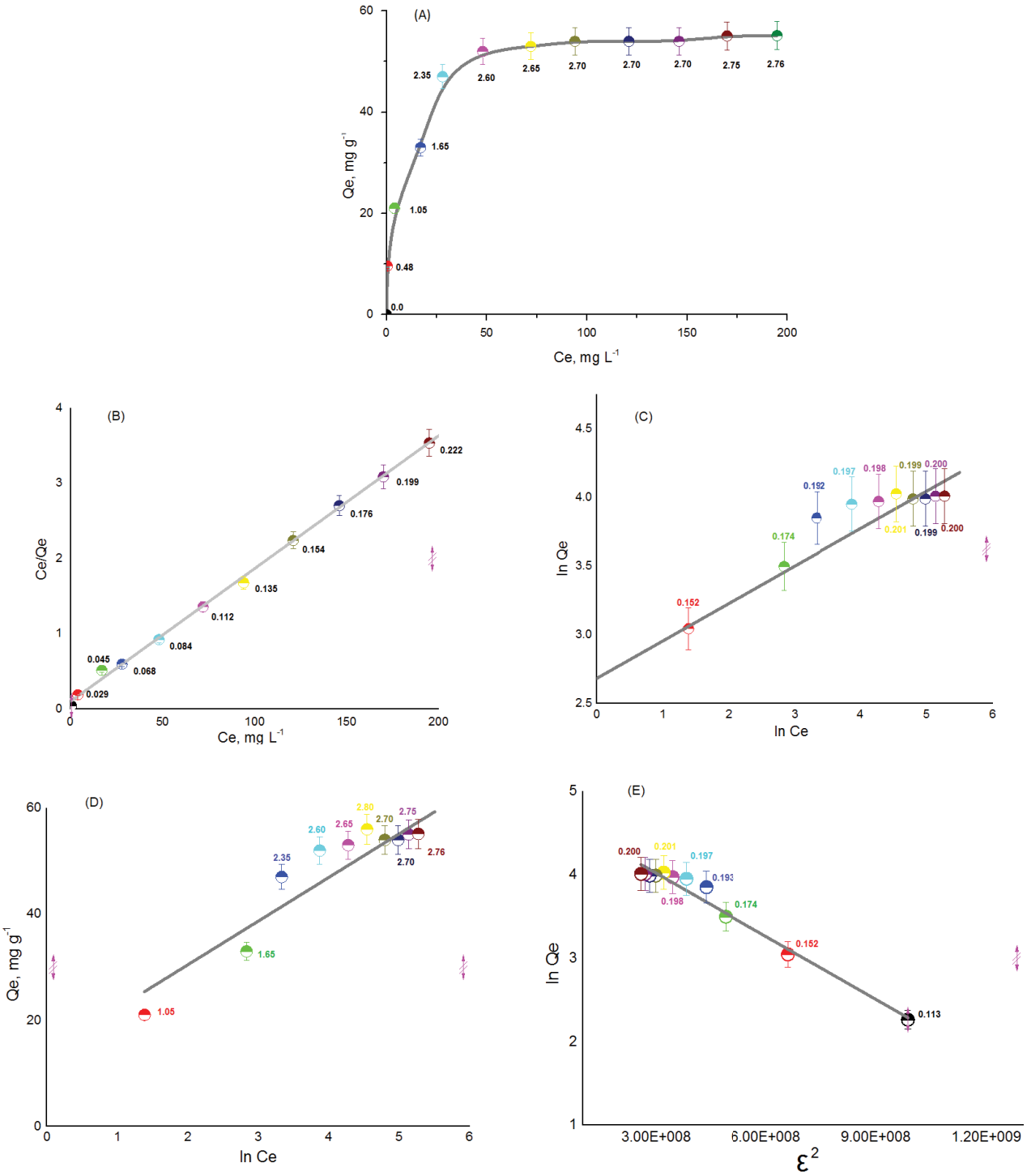

Fig. 10. (A) Adsorption isotherm of phosphate removal with PAni/BP composite: Initial $H_2PO_4^-$ concentration: 1.0–200 mg·L^{-1}, pH = 5.5, sample volume: 20 mL, adsorbent amount: 0.1 g, shaking time: 60 min, 25°C. Plotting of Langmuir (B) and Freundlich (C) isotherm models. Plotting of Temkin (D) and Dubinin–Radushkevich (E) isotherm models.

0.18 L·mg^{-1}, respectively. The Freundlich constant K_F was 0.51 L·g^{-1}, which shows a stronger affinity of the sorbent towards phosphate. The value of the n constant was higher than one (n = 1.20), which indicated the adsorbent has a greater affinity for phosphate. The values of both constants indicated a favorable and feasible phosphate adsorption process to the PAni/BP composite.

When neglecting the lower concentrations, the Temkin isotherm model showed a relevant correlation (R^2 = 0.851), Also, the value of the constant A_T indicated chemical

Table 4
Adsorption isotherm parameters for phosphate (5.0 mg·L^{-1} KH_2PO_4, pH 5.5) onto BP/PAni composite

Isotherm model	Parameter	
Experimental	Q_{max}, mg·g^{-1}	55.2
	Q_{max}, mg·g^{-1}	56.8
Langmuir model	K_L, L·mg^{-1}	0.18
	R^2	0.998
	n	1.20
Freundlich model	K_F	0.51
	R^2	0.967
	B, J·mol^{-1}	8.2
Temkin model	A_T	5.5
	R^2	0.851
	X_m, mol·g^{-1}	117.9
Dubinin–Radushkevich model	β, mol^2·J^{-2}	-2.52×10^{-9}
	E, kJ·mol^{-1}	14.1
	R^2	0.968

adsorption and the B constant was 8.2 J·mol^{-1}. Moreover, the positive B values indicated the adsorption is an endothermic process. The Dubinin–Radushkevich model showed a positive E value of 14.1 kJ·mol^{-1}, emphasizing an endothermic chemisorption process. These findings follow the results obtained from the pseudo-second-order kinetic and Langmuir isotherm models.

3.2.4. Adsorption mechanism

At the recommended adsorption pH 5.5, the dominant phosphate species is $H_2PO_4^-$ which has two P–OH groups serving as hydrogen bond donors and two hydrogen acceptors, P–O– and P=O. These groups can bind to the adsorbent via electrostatic attraction and hydrogen bonding forces. At pH ≤ pH_{zpc} = 5.3, electrostatic attraction originates as the adsorbent surface is positively charged, which means the NH groups of PAni and the OH and COOH groups of BP are present mainly in the protonated form, in addition to a lesser extent of the non-protonated form. Thus, electrostatic attraction forces of the negatively charged $H_2PO_4^-$ to the NH^+ groups in PAni, as well as the OH^+ and $COOH^+$ in BP, dominate the adsorption forces. In addition, to a lesser extent, the intermolecular hydrogen bonding occurs with the NH groups in the PAni part and the OH and COOH groups in the BP part. Once the pH is higher than 5.3, electrostatic attraction disappears as the adsorbent surface becomes negatively charged due to ionized OH and COOH groups in BP, reducing the electrostatic charges. According to Fig. 7A, removal remained high up to pH 6, indicating the hydrogen bonding became dominant but could not cause strong adsorption, leading to a steady decrease in the removal. Finally, the main adsorption mechanism is the electrostatic attraction, as shown in Fig. 11.

3.2.5. Adsorbent dosage

Small adsorbent dosages result in a low removal rate, whereas a larger amount of adsorbent provides more

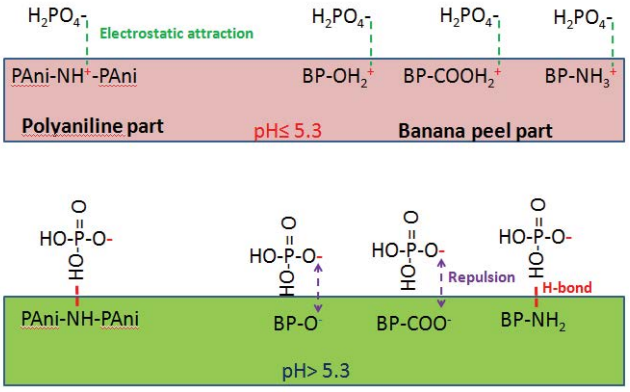

Fig. 11. Proposed adsorption mechanism of $H_2PO_4^-$ to PAni/BP composite.

adsorption sites that cannot be saturated [55]. The study of the effect of adsorbent dosage on the removal effect is extremely important economically. As shown in Fig. 12, the effect of adsorbent dosage on phosphate removal was investigated in the range of 0.5 to 5.0 g·L^{-1}. It was observed that adsorbent dosage has a strong influence on both the removal efficiency (%) and the adsorbed amount (Q_e).

As the adsorbent dosage was increased, the removal rate increased, whereas Q_e showed a steady decline. The removal rate exceeded 90% at a 1.5 g·L^{-1} adsorbent dose and continued to increase at higher dosages. The optimal dosage amount is taken at the intersection of both curves. Therefore, the best adsorbent dosage was 0.85 g·L^{-1}.

3.2.6. Desorption and reusability

To apply the developed composite for the removal from large sample volumes, it is necessary to investigate desorption. It was not possible to measure the phosphate in the supernatant after the adsorption process due to the low concentration below the detection limit of the quantification method.

Desorption was examined using varying concentrations of sodium hydroxide solution in the range of 0.05–1.0 mol·L^{-1}. According to Eq. (12), the desorption (%) was calculated.

$$\text{Desorption}\,(\%) = \frac{\text{Desorbed phosphate}\,(\text{mg})}{\text{Adsorbed phosphate}\,(\text{mg})} \quad (12)$$

Desorption gradually increased with increasing eluent concentration and reached a maximum removal of 92% at 0.15 mol·L^{-1}. Further concentrations of sodium hydroxide showed no improvement in the removal. Thus, a concentration of 0.15 mol·L^{-1} was recommended for phosphate desorption.

The reusability of PAni/BP was determined by measuring the adsorption (%), desorption (%), and adsorption capacity (Q_e) during ten consecutive adsorption–desorption experiments. The same dosage of the composite was used in a 5.0 mg·L^{-1} phosphate solution. Adsorption (%) fell by 2.9%, from 92.0% to 89.1%, while desorption (%) fell by 2.9%, from 91.5% to 66.4%. Results indicated no dramatic change

in the adsorption capacity after 10 cycles, it decreased by about 1.7%. This demonstrated that the composite could be recycled and used again for up to 10 cycles without losing its efficiency. As a result, the current adsorbent outperformed other green adsorbents in terms of durability, as presented in Table 1. This validated the structural stability and usability of the developed composite by confirming the chemical bonding between the PAni polymer and the BP surface and preventing further loss of active groups.

3.3. Biodegradability test

The biodegradability of the PAni/BP composite in freshwater was determined using the modified reported method [56] and the weight loss as a biodegradability index over 30 d (Fig. S2). In this context, the freshwater sample was obtained from a natural lake and used to test the biodegradability. The sample was applied just after being collected for no longer than 1 d. Also, the groundwater sample (G ≠ 4) was comparatively tested to investigate its biodegradation effect. Portions of 250 mL of freshwater and groundwater were transferred to glass containers, each containing 1.0 g of PAni/BP powder that was precisely weighed and documented as the initial weight (w_o) and was maintained immersed in water. The containers were then closed with cotton plugs and incubated in the dark under occasional shaking at 200 rpm and 25°C. After three weeks, the material was cleaned with double-distilled water and then dried at 60°C for 24 h. The weight of the remaining material (w) was measured. According to Bagheri et al. [57], the degradability (%) as a percentage of weight loss was calculated using the following Eq.13.

$$\text{Degradability}(\%) = \left[\frac{(w_o - w)}{w_o}\right] \times 100 \quad (13)$$

The sample's original mass is decreased to 0.91 and 0.86 g for freshwater and groundwater, respectively, corresponding to 9% and 14% degradability. It can be concluded that the produced adsorbent, which can be used to remove phosphate from natural water, can be less than 10% biodegradable after a month in freshwater. The bacteria and fungi present in freshwater could be the cause of biodegradation. Notably, some fungus started to appear on the adsorbent surface, indicating that more fungus grew. There is no doubt that the biodegradability of the soil/compost burial method would be expected to be higher than the applied freshwater method due to the greater number of fungi and bacteria present, thus accelerating the rate of mass loss.

To prove the activity of the developed composite over time, 20 mL volumes of distilled water and groundwater (G3) containing 0.1 g of PAni/BP, were used as models. The medium was then adjusted to a pH of 5.5 and incubated at 25°C for intervals of 0 to 4 d. After the predetermined time had passed, the mixture was spiked to 5.0 mg·L^{-1} of KH_2PO_4, and was then shaken for 60 min. The concentration of the remaining phosphate was measured to assess the removal (%). A supplemental Fig. S3 shows an image of the remaining phosphate molybdenum blue color obtained during the experiment investigation. As shown in Fig. 13, the removal after distilled water incubation remained constant after a day of incubation, whereas the activity in groundwater decreased by more than 10%. After 4 d of incubation, the adsorbent activity of distilled water and groundwater decreased by 19.4% and 15.2%, respectively, demonstrating that the material stability was affected by the added acid in the early stages but returned to a relatively constant level later. The degradability of the composite may be the cause of the higher activity loss. It's worth noting that the phosphate removal difference between distilled water and groundwater remained within 4% from the second to the fourth day. This demonstrates that the co-existence of ions did not cause a significant activity decline, but that it could have been caused by degradation.

3.4. Adsorption thermodynamic

The effect of temperature on the KH_2PO_4 (5.0 mg·L^{-1}, pH 5.5) adsorption and desorption (10 mL, 0.1 mol·L^{-1} NaOH)

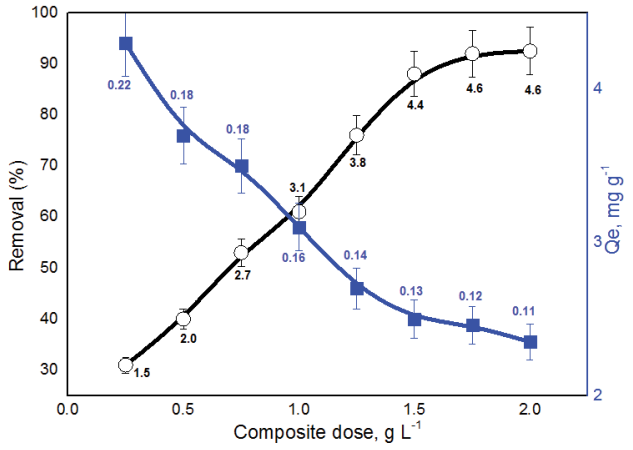

Fig. 12. Effect of composite dosage on the removal efficiency and adsorbed amount of phosphate by PAni/BP composite: initial $H_2PO_4^-$ concentration: 5.0 mg·L^{-1}, pH = 5.5, sample volume: 20 mL, shaking time: 60 min, 25°C.

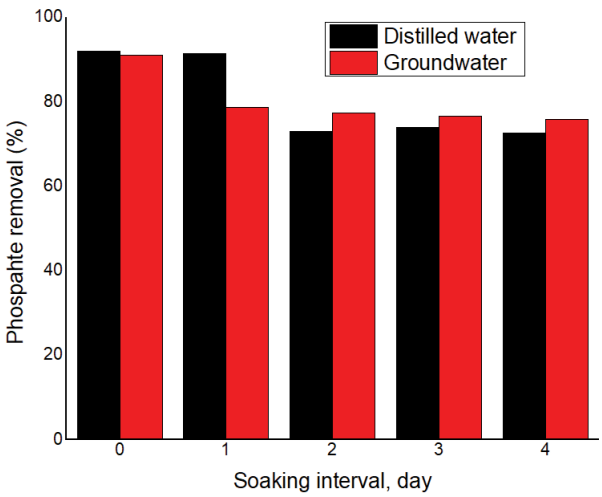

Fig. 13. Activity of PAni/BP composite over time at pH 5.5 after soaking in double-distilled water and groundwater (G3).

was studied from 20°C to 50°C. The results obtained are illustrated in Fig. 14A. The removal (%) marginally increased from 92.4% to 97.6% when the temperature was raised from 20°C to 50°C. This might be because endothermic adsorption is favored at higher temperatures.

Similarly, the desorption (%) increased from 92% to 96.8% with rising temperature due to the increase in the kinetic energy of adsorbed phosphate. The thermodynamic parameters characterize the thermodynamic feature of phosphate adsorption on the PAni/BP composite. The values of Gibb's free energy (ΔG), enthalpy (ΔH), and entropy (ΔS) were determined using Eqs. (14)–(16).

$$\Delta G^\circ = -RT\ln K_d \tag{14}$$

$$\Delta G^\circ = \Delta H^\circ - T\Delta S^\circ \tag{15}$$

$$\ln K_d = \frac{\Delta S^\circ}{R} - \frac{\Delta H^\circ}{RT} \tag{16}$$

where K_d is the distribution constant at absolute temperature T (K), and R is the universal gas constant (8.314 J·mol^{-1}·K^{-1}). The K_d is calculated by dividing the amount of phosphate adsorbed (Q_e) by the equilibrium concentration (C_e). The plot of lnK_d against 1/T is shown in Fig. 14B.

Thermodynamic parameters obtained are presented in Table 5. The negative ΔG° values, which range from –9.5 to –7.5 kJ·mol^{-1}, signify spontaneous adsorption. The positive value of ΔH° revealed endothermic adsorption [58]. Moreover, the increase in phosphate ion randomness at the adsorbent-solution interface and the significant phosphate ion affinity for the PAni/BP composite were both indicated by the positive value of ΔS°. These outcomes are similar to the reported values of other composites, including chitosan/bentonite [42] and graphene oxide/Fe_3O_4 [59].

3.5. Effect of co-existing ions

Other possible co-existing ions like Na^+, Ca^{2+}, Mg^{2+}, Fe^{3+}, Mn^{2+}, Cu^{2+}, Pb^{2+}, Cl^-, SO_4^-, and NO_3^-, as well as dyes like methyl orange and rhodamine B, were examined for their potential interference. In every case, the phosphate (K_2HPO_4) concentration stayed constant at 5.0 mg·L^{-1}. In double-distilled water, binary mixtures of the interfering ion and the phosphate were prepared, and under optimal adsorption circumstances, the removal (%) was calculated. According to the findings shown in Table 6, the error (%) was lower than 3% in the presence of all species except Cl^-, SO_4^-, and methyl orange. Chloride and sulfate removal (%) increased by 6.2% and 4.1%, respectively, which may have been caused by a reduction in the diffusion layer due to an increase in ionic strength [13]. Additionally, methyl orange dye significantly decreased removal due to competition for positive adsorption sites in the composite and the dye's ability to bind via hydrophobic–hydrophobic interaction.

3.6. Application to groundwater

Table 2 shows the effectiveness of phosphate removal by PAni/BP composite in untreated groundwater as a function of all physico-chemical factors. The groundwater sample was spiked with 10 mg·L^{-1} of KH_2PO_4 to suit the detection limit of the employed determination method. The remained amount of phosphate was measured, and the removal (%)

Table 5
Thermodynamic parameters of phosphate (5.0 mg·L^{-1} KH_2PO_4, pH 5.5) adsorption onto PAni/BP composite

ΔS°, kJ·mol^{-1}·K^{-1}	ΔH°, kJ·mol^{-1}	ΔG°, kJ·mol^{-1}	Temperature, K
293	–7.5		
303	–8.1		
308	–8.5	–12.1	0.067
313	–8.8		
318	–9.1		
323	–9.5		

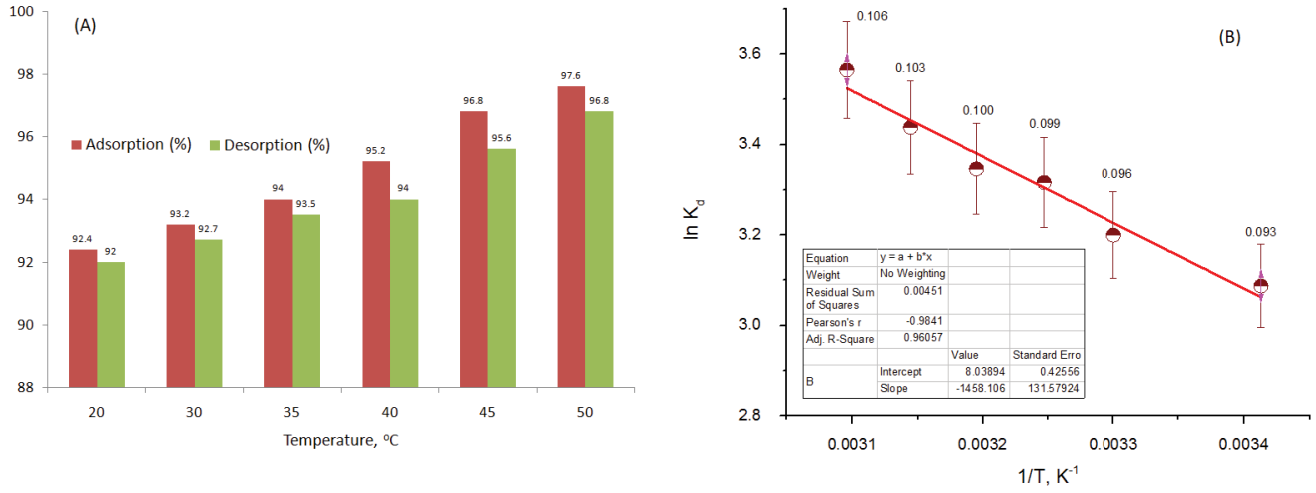

Fig. 14. (A) Effect of temperature on the adsorption–desorption of phosphate (5.0 mg·L^{-1} KH_2PO_4), 0.1 g BP/PAni at pH 5.5. (B) Plot of lnK_d vs. 1/T.

was assessed. For G1, G2, G3, G4, and G5, the phosphate removal was 95, 90, 91, 93, and 90%, correspondingly. The removal (%) was also investigated using phosphate desorption after groundwater was spiked to levels of 0, 3, and 5.0 mg·L^{-1}, and the results are shown in Table 7. The removal (%) ranged from 92%–100% to 84%–90%, 87%–95% to 84%–91%, and 83%–88% for G1, G2, G3, G4, and G5, respectively. The obtained results were comparative, indicating that the composite successfully resisted the elevated levels of TDS in groundwater. However, the sample G1 with TDS in the drinking water range (202 mg·L^{-1}) had the best removal efficacy, where it reached 100%. This demonstrates that the sample was polluted with phosphate and that, under these conditions, PAni/BP was able to adsorb the contamination. Furthermore, the corresponding relative standard deviation (n = 5) ranged from 2.0%–7.4%, which are considered satisfactory results (less than 10%), confirming the accuracy of the obtained results. It is worth noting that the majority of the removal (%) ranged between 80% and 90%, indicating that some of the anions were encountered with the added phosphate anions. Despite this, the developed adsorbent can be considered efficient for phosphate removal from complex matrices waters because the added phosphate and TDS levels examined are higher than those found in most natural waters.

Table 6
Interfering effect of co-existing ions and dyes on the removal of phosphate (5.0 mg·L^{-1} KH_2PO_4, pH 5.5) by PAni/BP composite

Co-existing ion	Concentration added, mg·L^{-1}	Removal (%)	Error (%)
–	–	92.0	–
Na^+	1,000	92.4	+0.4
Ca^{2+}	500	91.5	–0.5
Mg^{2+}	200	91.0	–1.0
Fe^{3+}	2.0	92.8	+0.8
Mn^{2+}	2.0	90.0	–2.0
Pb^{2+}	0.1	92.5	+0.5
Cu^{2+}	0.1	90.7	–1.3
Cl^-	1,000	98.2	+6.2
SO_4^-	500	96.1	+4.1
NO_3^-	20	91.3	–0.7
Methyl orange	5.0	87.4	–4.6
Rhodamine B	5.0	90.8	–1.2

As previously stated, the primary goal of phosphate adsorbents is to have a greater adsorption capacity at low phosphate concentrations. Therefore, the influence of sample volume was examined to study the impact of dilution or lowering the initial concentration on the phosphate adsorption efficiency. The volume of groundwater examined for the removal efficiency was in the range of 20–500 mL, with an added phosphate concentration of 2.0 mg·L^{-1} and a composite dose of 0.1 g·L^{-1}. Fig. 15 depicts the obtained results. The removal decreased from 90%–82%, 89%–84%, 91%–95%, 88%–76%, and 89%–78% for G1, G2, G3, G4 and G5, respectively.

Except for G ≠ 4, which had a higher salinity than the other samples, the decrease was less than 10% for all samples. As a result, 250 mL was deemed the breakthrough volume for qualitative removal. The decrease in removal efficiency could be attributed to the leaching effect of the solvent on the adsorbed phosphate, resulting in desorption from the composite surface. Using an eluent volume of 5.0 mL from a 0.15 mol·L^{-1} sodium hydroxide solution, the preconcentration factor was calculated by dividing the sample volume by the eluate volume and was found to be 50. This also allows for the removal and quantification of phosphate in real-world waters at levels ranging from low to high concentrations.

Table 7
Recovery data of phosphate from groundwater samples using the PAni/BP composite (n = 5)

Groundwater	Initial PO_4^- concentration, mg·L^{-1}	PO_4^- added, mg·L^{-1}	Found (mean ± SD), mg·L^{-1}	Removal (%)	Relative standard deviation (%)
		0.0	1.83 ± 0.06	92	3.3
G ≠ 1	2.0	3.0	4.98 ± 0.21	99	4.2
		5.0	5.0 ± 0.47	100	9.4
		0.0	0.98 ± 0.02	89	2.0
G ≠ 2	1.1	3.0	3.79 ± 0.12	90	3.2
		5.0	5.28 ± 0.30	84	5.7
		0.0	1.60 ± 0.04	89	2.5
G ≠ 3	1.8	3.0	4.42 ± 0.26	87	5.9
		5.0	6.55 ± 0.29	95	4.4
		0.0	2.10 ± 0.14	91	6.7
G ≠ 4	2.3	3.0	4.92 ± 0.35	87	7.1
		5.0	6.51 ± 0.47	84	7.2
		0.0	2.28 ± 0.15	88	6.6
G ≠ 5	2.6	3.0	5.10 ± 0.27	83	5.3
		5.0	6.85 ± 0.20	85	2.9

Table 8
Comparison of the adsorption properties of PAni/BP composite for phosphate adsorption with other reported composites

Composite	Sample	Adsorption capacity, $mg \cdot g^{-1}$	Equilibration time, min	Temperature, °C	pH	Removal (%)	Re-use cycles	References
PAni/BPa	Groundwater	56.8	60	25	5.5	83–100	10	This work
Al/bentonite	Aqueous media	4.64	360	25	3.0	>90	–	[60]
PANi/Lab	Environmental water	45.24	150	–	4.0	>90	3.0	[30]
Zr- chitosan/bentonite	Water	65.39	10	25	5.0	–	–	[42]
Polyaniline/$Ni_{0.5}Zn_{0.5}Fe_2O_4$	Water resources	85.4	30	25	5.0	90.3	–	[48]
MFC@UiO-66c	Water	9.9	180	25	6.5	>80	5.0	[61]
Polyaniline/TiO_2	Wastewater	12.1	60	25	6.0	95	8.0	[45]
La/activated carbon	Physiological samples	15.43	48 h	37	7.8	–	–	[50]
Fe-Cu/fly ash	Wastewater	12.7	120	25	–	97.97	–	[62]

[a]Polyaniline/banana peel;
[b]Lanthanum;
[c]Magnetic ferrite core–shell composite/metal–organic framework (UiO-66).

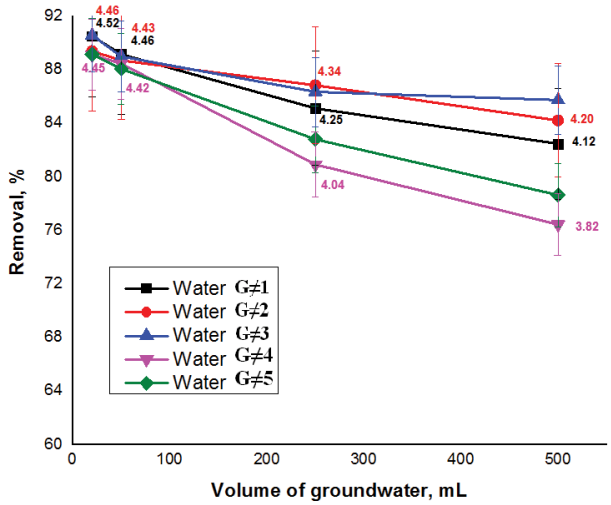

Fig. 15. Effect of volume of groundwater on the removal of phosphate by PAni/BP composite: added phosphate concentration of 2.0 $mg \cdot L^{-1}$, solution pH 5.5, and shaking time of 60 min.

4. Comparison to other adsorbents

Table 8 shows a comparison of the adsorption capacity, optimal solution pH, equilibration time, and reusability of the present PAni/BP composite with other reported phosphate sorbents. The adsorption capacity of the developed sorbent was found to be higher than that of aluminum/bentonite [59], polyaniline/lanthanum [30], magnetic ferrite carbon-core/metal–organic framework (MFC@UiO-66) [61], lanthanum/activated carbon [50], and Fe-Cu bimetallic modified fly ash [62]. In contrast, other sorbents such as chitosan/bentonite [42] and polyaniline/$Ni_{0.5}Zn_{0.5}Fe_2O_4$ [48] showed higher capacities than PAni/BP. The optimal pH was comparable to that of other adsorbents [42,45,48], suggesting that the mechanisms for adsorption were similar. Phosphate transferred to PAni/BP faster and with greater strength, as evidenced by the fact that the equilibration time was shorter than that of several other adsorbents. Despite this, other characteristics such as low cost, ease of preparation, and tolerance to higher TDS waters make this material suitable for the adsorption and removal of phosphate in diverse water samples. This proves the proposed material is a viable option for removing phosphate from water samples, even in complex matrices. This also confirms the efficacy of using this material in real applications.

5. Conclusions

The present work explores the application of an environmentally-safe adsorbent obtained from BP and PAni as an alternative to costly adsorbents for the removal of phosphate from water samples. The FT-IR spectra showed the chemical bonding between the BP and PAni surface groups. The XRD pattern revealed the amorphous crystallinity typical for non-crystalline structures. The SEM micrograph indicated the smoothing of the surface after the incorporation of PAni into BP. TGA analysis showed good thermal stability of the PAni/BP composite against oxidative decomposition. The BET data indicated a high surface area of 5.65 $m^2 \cdot g^{-1}$ and a pore size of 61.2 nm. The removal rate was found to be fast and reached equilibration after 40 min due to the rapid accumulation of phosphate on the composite surface. The optimal pH of 5.5 revealed the electrostatic attraction of the negatively charged $H_2PO_4^-$ to the positively charged composite surface containing the protonated OH_2^+, NH_3^+, $COOH_2^+$, and $-^+NH=$ groups. The adsorption mechanism obeyed the pseudo-second-order and Langmuir isotherm models, confirming chemical adsorption. Adsorbent capacity was found to be 56.8 $mg \cdot g^{-1}$ which is greater than several other reported adsorbents for phosphate removal. Only 9% of the developed composite's weight was lost over 30 d in freshwater, indicating low biodegradability. The thermodynamic

parameters confirmed the spontaneous and endothermic adsorption process. The cyclicity of the adsorbent was found feasible after ten adsorption–desorption experiments. Application to groundwater with a wide TDS range from 202 to 3,040 mg·L^{-1} showed removal efficiency ≥83%. Thus, PAni/BP has proven to be a promising material for the removal of phosphate from an aqueous solution. The above-findings make the developed procedure an alternative for adsorptive removal in groundwater samples with low-cost adsorbent.

Acknowledgment

The authors extend their appreciation to the deanship of scientific research at Shaqra University for funding this research work through project number (SU-ANN-202222).

CRediT authorship contribution statement

Abdullah A. Alotaibi: Conceptualization, Resources, Supervision, Review & editing.

Abdulrahman F. Alharbi: Characterization tests and results interpretation.

Ahmed M.H. Ibrahim: Investigation, Methodology, Formal analysis.

Sami M. Abdel Azeem: Conceptualization, Data curation, Writing – review & editing, Project administration, Funding acquisition.

Declaration of interest

The authors declare no potential conflict of interest.

References

[1] M. Jiang, Y. Yang, T. Lei, Z. Ye, S. Huang, X. Fu, P. Liu, H. Li, Removal of phosphate by a novel activated sewage sludge biochar: equilibrium, kinetic and mechanism studies, Appl. Energy Combust. Sci., 9 (2022) 100056, doi: 10.1016/j.jaecs.2022.100056.

[2] L. Fang, W. Zeng, L. Xu, L.Z. Huang, Green rusts as a new solution to sequester and stabilize phosphate in sediments under anoxic conditions and their implication for eutrophication control, Chem. Eng. J., 388 (2020) 124198, doi: 10.1016/j.cej.2020.124198.

[3] G. Fan, L. Hong, J. Luo, Y. You, J. Zhang, P. Hua, B. Du, J. Zhan, R. Ning, M. Bao, Photocatalytic inactivation of harmful algae and degradation of cyanotoxins microcystin-LR using GO-based Z-scheme nanocatalysts under visible light, Chem. Eng. J., 392 (2020) 123767, doi: 10.1016/j.cej.2019.123767.

[4] S. Fried, B. Mackie, E. Nothwehr, Nitrate and phosphate levels positively affect the growth of algae species found in Perry Pond, Tillers, 4 (2003) 21–24.

[5] I.W. Almanassra, Go. Mckay, V. Kochkodan, M.A. Atieh, T. Al-Ansari, A state of the art review on phosphate removal from water by biochars, Chem. Eng. J., 409 (2021) 128211, doi: 10.1016/j.cej.2020.128211.

[6] H. Yan, Q. Chen, J. Liu, Y. Feng, K. Shih, Phosphorus recovery through adsorption by layered double hydroxide nano-composites and transfer into a struvite-like fertilizer, Water Res., 145 (2018) 721–730.

[7] W. Huang, Y. Zhang, D. Li, Adsorptive removal of phosphate from water using mesoporous materials: a review, J. Environ. Manage., 193 (2017) 470–482.

[8] S.M. Abdel Azeem, M.M.S. Wahsh, F.H. Youssef, A.M.H. Ibrahim, N. Burham, Magnetic nanocomposite of zinc–manganese ferrite/polyurethane foam for adsorption of copper and cadmium from water, Desal. Water Treat., 267 (2022) 26–44.

[9] X. Xu, Y. Gao, B. Gao, X. Tan, Y.-Q. Zhao, Q. Yue, Y. Wang, Characteristics of diethylenetriamine-crosslinked cotton stalk/wheat stalk and their biosorption capacities for phosphate, J. Hazard. Mater., 192 (2011) 1690–1696.

[10] C. Namasivayam, D. Sangeetha, Equilibrium and kinetic studies of adsorption of phosphate onto $ZnCl_2$ activated coir pith carbon, J. Colloid Interface Sci., 280 (2004) 359–365.

[11] Y. Shang, K. Guo, P. Jiang, X. Xu, B. Gao, Adsorption of phosphate by the cellulose-based biomaterial and its sustained release of laden phosphate in aqueous solution and soil, Int. J. Biol. Macromol., 109 (2018) 524–534.

[12] X. Xu, B.-Y. Gao, Q.-Y. Yue, Q.-Q. Zhong, Preparation of agricultural by-product based anion exchanger and its utilization for nitrate and phosphate removal, Bioresour. Technol., 101 (2010) 8558–8564.

[13] A. Robalds, L. Dreijalte, O. Bikovens, M. Klavins, A novel peat-based biosorbent for the removal of phosphate from synthetic and real wastewater and possible utilization of spent sorbent in land application, Desal. Water Treat., 57 (2016) 13285–13294.

[14] P. Paul, S. Parbat, G. Aditya, Phosphate ion removal from aqueous solution using snail shell dust: biosorption potential of waste shells of edible snails, RSC Adv., 12 (2022) 30011, doi: 10.1039/d2ra03852h.

[15] S.Y. Lee, J.-W. Choi, K.G. Song, K. Choi, Y.J. Lee, K.-W. Jung, Adsorption and mechanistic study for phosphate removal by rice husk-derived biochar functionalized with Mg/Al-calcined layered double hydroxides via co-pyrolysis, Composites, Part B, 176 (2019) 107209, doi: 10.1016/j.compositesb.2019.107209.

[16] Y.-Y. Wang, H.-H. Lu, Y.-X. Liu, S.-M. Yang, Removal of phosphate from aqueous solution by SiO_2–biochar nanocomposites prepared by pyrolysis of vermiculite treated algal biomass, RSC Adv., 6 (2016) 83534–83546.

[17] Q.Y. Yue, W.-Y. Wang, B.-Y. Gao, X. Xu, J. Zhang, Q. Li, Phosphate removal from aqueous solution by adsorption on modified giant reed, Water Environ. Res., 82 (2010) 374–381.

[18] Q. Yin, B. Zhang, R. Wang, Z. Zhao, Phosphate and ammonium adsorption of sesame straw biochars produced at different pyrolysis temperatures, Environ. Sci. Pollut. Res., 25 (2018) 4320–4329.

[19] A. Folino, A. Karageorgiou, P.S. Calabrò, D. Komilis, Biodegradation of wasted bioplastics in natural and industrial environments: a review, Sustainability, 12 (2020) 6030, doi: 10.3390/su12156030.

[20] M.N. Piol, C. Dickerman, M.P. Ardanza, A. Saralegui, S.P. Boeykens, Simultaneous removal of chromate and phosphate using different operational combinations for their adsorption on dolomite and banana peel, J. Environ. Manage., 288 (2021) 112463, doi: 10.1016/j.jenvman.2021.112463.

[21] R. Foroutan, S.J. Peighambardoust, R. Mohammadi, S.H. Peighambardoust, B. Ramavandi, Cadmium ion removal from aqueous media using banana peel biochar/Fe_3O_4/ZIF-67, Environ. Res., 211 (2022) 113020, doi: 10.1016/j.envres.2022.113020.

[22] A.A. Oladipo, E. Od. Ahaka, M. Gazi, High adsorptive potential of calcined magnetic biochar derived from banana peels for Cu^{2+}, Hg^{2+}, and Zn^{2+} ions removal in single and ternary systems, Environ. Sci. Pollut. Res., 26 (2019) 31887–31899.

[23] R.T. Kapoor, M. Rafatullah, M.R. Siddiqui, M.A. Khan, M. Sillanpää, Removal of Reactive black 5 dye by banana peel biochar and evaluation of its phytotoxicity on tomato, Sustainability, 14 (2022) 4176, doi: 10.3390/su14074176.

[24] A. Li, H. Deng, Y. Wu, C. Ye, Y. Jiang, Strong adsorption of phosphorus by ZnAl-LDO-activated banana biochar: an analysis of adsorption efficiency, thermodynamics, and internal mechanisms, ACS Omega, 6 (2021) 7402–7412.

[25] A. Samadi, M. Xie, J. Li, H. Shon, C. Zheg, S. Zhao, Polyaniline-based adsorbents for aqueous pollutants removal: a review, Chem. Eng. J., 418 (2021) 129425, doi: 10.1016/j.cej.2021.129425.

[26] T.C. Maponya, M.J. Hato, T.R. Somo, K.E. Ramohlola, M.D. Mokhafola, G.R. Monama, A. Maity, K.D. Modibane,

L.M. Katata-Seru, Polyaniline-based nanocomposites for environmental remediation, in, heavy metal ions removal, InTechOpen, 2019, doi: 10.5772/intechopen.82384.
[27] E.N. Zare, A. Motahari, M. Sillanpaa, Nanoadsorbents based on conducting polymer nanocomposites with main focus on polyaniline and its derivatives for removal of heavy metal ions/dyes: a review, Environ. Res., 162 (2018) 173–195.
[28] S. Mondal, U. Rana, P. Das, S. Malik, Network of polyaniline nanotubes for wastewater treatment and oil/water separation, ACS Appl. Polym. Mater., 1 (2019) 1624–1633.
[29] H. Hajjaoui, A. Soufi, W. Boumya, M. Abdennouri, N. Barka, Polyaniline/nanomaterial nanocomposites for the removal of heavy metals by adsorption: a review, J. Compos. Sci., 5 (2021) 233, doi: 10.3390/jcs5090233.
[30] S. Rezania, A. Kadi, H. Kamyab, A.A. Ghfar, H.R. Nodeh, W.N.W. Ibrahim, Lanthanum doped magnetic polyaniline for removal of phosphate ions from water, Chemosphere, 307 (2022) 135809, doi: 10.1016/j.chemosphere.2022.135809.
[31] M. Duhan, R. Kaur, Nano-structured polyaniline as a potential adsorbent for methylene blue dye removal from effluent, J. Compos. Sci., 5 (2021) 7, doi: 10.3390/jcs5010007.
[32] K. Rachna, A. Agarwal, N.B. Singh, Preparation and characterization of zinc ferrite—polyaniline nanocomposite for removal of Rhodamine B dye from aqueous solution, Environ. Nanotechnol. Monit. Manage., 9 (2018) 154–163.
[33] M. Li, F. Sun, W. Shang, X. Zhang, W. Dong, Z. Dong, S. Zhao, Removal mechanisms of perfluorinated compounds (PFCs) by nanofiltration: roles of membrane-contaminant interactions, Chem. Eng. J., 406 (2021) 126814, doi: 10.1016/j.cej.2020.126814.
[34] F. Ishtiaq, H.N. Bhatti, A. Khan, M. Iqbal, A. Kausar, Polypyrole, polyaniline and sodium alginate biocomposites and adsorption–desorption efficiency for imidacloprid insecticide, Int. J. Biol. Macromol., 147 (2020) 217–232.
[35] F. Mashkoor, A. Nasar, Polyaniline/*Tectona grandis* sawdust: a novel composite for efficient decontamination of synthetically polluted water containing crystal violet dye, Groundwater Sustainable Dev., 8 (2019) 390–401.
[36] S.G. Mohammad, D.E. Abulyazied, S.M. Ahmed, Application of polyaniline/activated carbon nanocomposites derived from different agriculture wastes for the removal of Pb(II) from aqueous media, Desal. Water Treat., 170 (2019) 199–210.
[37] Y. Liu, X. Sheng, Y. Dong, Y. Ma, Removal of high-concentration phosphate by calcite: effect of sulfate and pH, Desalination, 289 (2012) 66–71.
[38] W.M. Hikal, H.A.H. Said-Al Ahl, A. Bratovcic, K.G. Tkachenko, J. Sharifi-Rad, M. Kačániová, M. Elhourri, M. Atanassova, Banana peels: a waste treasure for human being, Evidence-Based Complementary Alternative Med., 2022 (2022) 7616452, doi: 10.1155/2022/7616452.
[39] A. Nasiri, S. Rajabi, M. Hashimi, CoFe2O4@methylcellulose/AC as a new, green, and eco-friendly nano-magnetic adsorbent for removal of Reactive red 198 from aqueous solution, Arabian J. Chem., 15 (2022) 103745, doi: 10.1016/j.arabjc.2022.103745.
[40] J. Murphy, J.P. Riley, A modified single solution for the determination of phosphate in natural waters, Anal. Chim. Acta, 27 (1962) 31–36.
[41] WHO, Guideline for Drinking-Water Quality, Vol. 1, 3rd ed., World Health Organization (WHO), Geneva, 2004.
[42] J. Wang, Y. Liu, P. Hu, R. Huang, Adsorption of phosphate from aqueous solution by Zr(IV)-crosslinked quaternized chitosan/bentonite composite, Environ. Prog. Sustainable Energy, 37 (2018) 267–275.
[43] Y.S. Ho, G. McKay, Sorption of dye from aqueous solution by peat, Chem. Eng. J., 70 (1998) 115–124.
[44] Y.S. Ho, G. Mckay, D.A.J. Wase, C.F. Forster, Study of the sorption of divalent metal ions on to peat, Adsorpt. Sci. Technol., 18 (2000) 639–650.
[45] W.J. Weber, J.C. Morris, Kinetics of adsorption on carbon from solution, J. Sanit. Eng. Div. ASCE, 89 (1963) 31–59.
[46] A.M. Osman, A.H. Hendi, T.A. Saleh, Simultaneous adsorption of dye and toxic metal ions using an interfacially polymerized silica/polyamide nanocomposite: kinetic and thermodynamic studies, J. Mol. Liq., 314 (2020) 113640, doi: 10.1016/j.molliq.2020.113640.
[47] Q. Li, H. Liu, T. Liu, M. Guo, B. Qing, X. Ye, Z. Wu, Strontium and calcium ion adsorption by molecularly imprinted hybrid gel, Chem. Eng. J., 157 (2010) 401–407.
[48] M.H. Tarmahi, F. Moeinpour, Phosphate removal from aqueous solutions using polyaniline/$Ni_{0.5}Zn_{0.5}Fe_2O_4$ magnetic nanocomposite, Environ. Health Eng. Manage. J., 4 (2017) 65–71.
[49] N. Wang, J. Feng, J. Chen, J. Wang, W. Yan, Adsorption mechanism of phosphate by polyaniline/TiO_2 composite from wastewater, Chem. Eng. J., 316 (2017) 33–40.
[50] R. Nazarian, R.J. Desch, S.W. Thiel, Kinetics and equilibrium adsorption of phosphate on lanthanum oxide supported on activated carbon, Colloids Surf., A, 624 (2021) 126813, doi: 10.1016/j.colsurfa.2021.126813.
[51] I. Langmuir, The adsorption of gases on plane surfaces of glass, mica and platinum, J. Am. Chem. Soc., 40 (1918) 1361–1403.
[52] H.M.F. Freundlich, Over the adsorption in solution, J. Phys. Chem., 57 (1906) 385–470.
[53] M. Kondalkar, U. Fegade, Inamuddin, S. Kanchi, T. Altalhi, K.E. Suryawanshi, A.M. Patil, Adsorption of Cr(VI) on ultrafine Al_2O_3-doped $MnFe_2O_4$ nanocomposite surface: experimental and theoretical study using double-layer modeling, J. Phys. Chem. Solids, 163 (2022) 110544, doi: 10.1016/j.jpcs.2021.110544.
[54] N.S. Ammar, N.A. Fathy, H.S. Ibrahim, S.M. Mousa, Micro-mesoporous modified activated carbon from corn husks for removal of hexavalent chromium ions, Appl. Water Sci., 11 (2021) 154, doi: 10.1007/s13201-021-01487-1.
[55] Y. Ma, Z. Deng, Z. Li, Q. Lin, Y. Wu, W. Dou, Adsorption characteristics and mechanism for $K_2Ti_4O_9$ whiskers removal of Pb(II), Cd(II), and Cu(II) cations in wastewater, J. Environ. Chem. Eng., 9 (2021) 106236, doi: 10.1016/j.jece.2021.106236.
[56] S. Sultana, N. Ahmad, S.M. Faisal, M. Owais, S. Sabir, Synthesis, characterisation and potential applications of polyaniline/chitosan-Ag-nano-biocomposite, IET Nanobiotechnol., 11 (2017) 835–842.
[57] N. Bagheri, M.M. Lakouraj, V. Hasantabar, M. Mohsen, Biodegradable macro-porous CMC-polyaniline hydrogel: synthesis, characterization and study of microbial elimination and sorption capacity of dyes from wastewater, J. Hazard. Mater., 403 (2021) 123631, doi: 10.1016/j.jhazmat.2020.123631.
[58] R.R. Kalantry, A.J. Jafari, A. Esrafili, B. Kakavandi, A. Gholizadeh, A. Azari, Optimization and evaluation of reactive dye adsorption on magnetic composite of activated carbon and iron oxide, Desal. Water Treat., 57 (2016) 6411–6422.
[59] L. Bai, L. Yuan, Y. Ji, H. Yan, Effective removal of phosphate from aqueous by graphene oxide decorated with α-Fe_2O_3: kinetic, isotherm, thermodynamic and mechanism study, Arabian J. Sci. Eng., 43 (2018) 3611–3620.
[60] L.G. Yan, Y.Y. Xu, H.Q. Yu, X.D. Xin, Q. Wei, B. Du, Adsorption of phosphate from aqueous solution by hydroxy-aluminum, hydroxy-iron and hydroxy-iron–aluminum pillared bentonites, J. Hazard. Mater., 179 (2010) 244–2450.
[61] T. Liu, S. Zheng, L. Yang, Magnetic zirconium-based metal–organic frameworks for selective phosphate adsorption from water, J. Colloid Interface Sci., 552 (2019) 134–141.
[62] K. Xu, H. Tao, T. Deng. Removal of phosphate from coating wastewater using magnetic Fe-Cu bimetal oxide modified fly ash, J. Water Reuse Desal., 6 (2016) 430–436.

Supporting information

Fig. S1. An image for the total dissolved solids measurement of the studied groundwater samples.

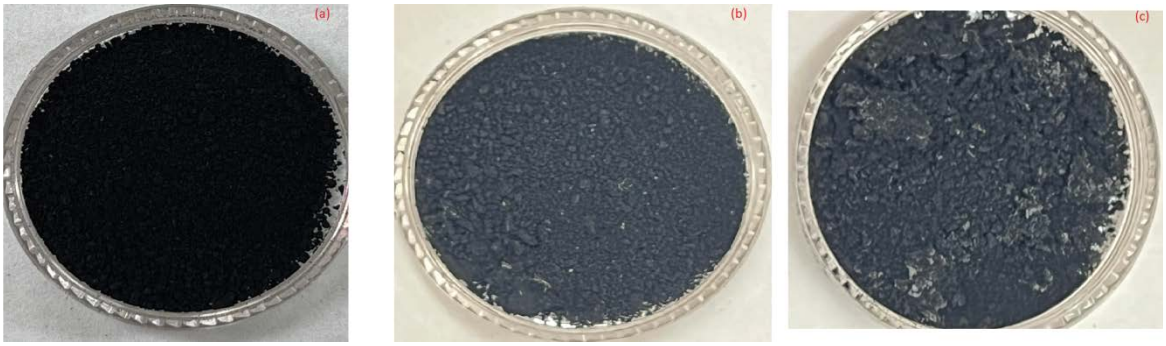

Fig. S2. Biodegradability test of PAni/BP composite. Images of the developed composite before biodegradation (a), and after 30 d in freshwater (b) and in 2,000 mg·L^{-1} groundwater (c).

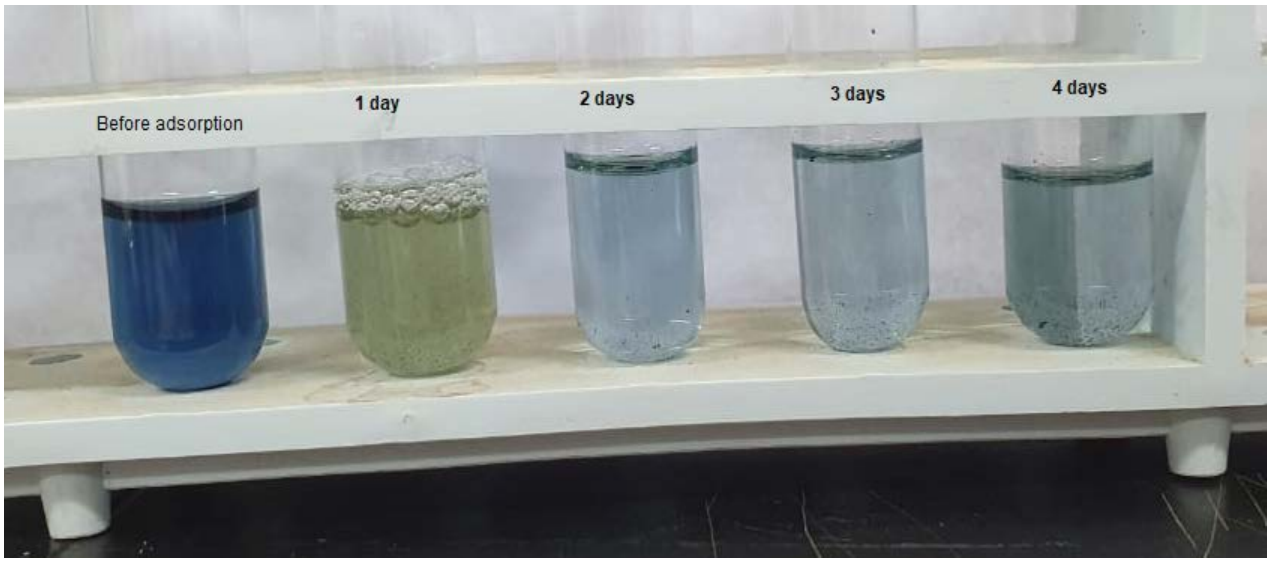

Fig. S3. An image of the remaining phosphate determined by the molybdenum blue method after various incubation intervals of PAni/BP adsorbent in double-distilled water at pH 5.5.